SUPPLEMENTAL MATERIALS

Reagents. Human thrombin, rabbit IgG, goat IgG, PGE1, rabbit polyclonal anti-PDI antibodies, quercetin-3-rutinoside (rutin), and Duolink® In Situ Red Proximity Ligation Assay Kit Goat/Rabbit were purchased from Sigma (St. Louis, MO). D-Phe-Pro-Arg-chloromethyl ketone (PPACK) was obtained from EMD Millipore (Billerica, MA). Human vWF was from Haematologic Technologies (Essex Junction, VT). Botrocetin was kindly provided by Robert Andrews (Monash University, Australia).[1] Ristocetin was purchased from American Biochemical & Pharmaceuticals Ltd (Marlton, NJ). Cell-impermeable, biotin-containing probes that react with primary amines (sulfo-N-hydroxysulfosuccinimide-biotin, SSB) or free thiol (N^{α}-(3-Maleimidylpropionyl) biocytin, MPB), Alexa Fluor 488-conjugated anti-His or anti-rat IgG antibodies, an Alexa Fluor 647-conjugated goat anti-mouse IgG1 antibody, mouse monoclonal anti-GPIbα (clone: MM2/174 & SZ2) antibodies, lipofectamine 2000 transfection reagent, calcein-AM dye, and protein A/G agarose beads were from Thermo Scientific (Rockford, IL). Monoclonal blocking anti-PDI (clone: BD34), anti-human GPIbα (clone: HIP1), anti-mouse P-selectin (clone: RB40.34) antibodies were obtained from BD Biosciences (San Jose, CA). Purified proteins of an ectodomain of human αMβ2 (αM: Phe17-Asn1105 and β2: Gln23-Asn700 expressed in CHO cells) and GPIbα (His17-Leu505 expressed in CHO cells), goat IgG, polyclonal goat anti-PDI, goat anti-human β2, and goat anti-PDI antibodies were from R&D Systems (Minneapolis, MN). GST-tagged full-length human GPIbα (Met1-Leu652 with a truncation of Pro406-Ala431, expressed in Wheat germ) was purchased from Creative BioMart Inc. (Shirley, NY). Rabbit polyclonal anti-vWF and anti-GPIbα antibodies were from Santa Cruz (Santa Cruz, CA). A rabbit polyclonal anti-PDI antibody was

obtained from Novus Biologicals (Littleton CO). Recombinant mouse TNF-α, an Alexa Fluor 647-conjugated antibody against mouse Ly-6G were purchased from BioLegend (San Diego, CA). FITC-conjugated rabbit polyclonal anti-vWF antibodies were obtained from Bioss antibodies (Woburn, MA). PE- or FITC-conjugated control IgGs or monoclonal antibodies against mouse P-selectin, activated αIIbβ3 integrin (clone: JON/A), or glycoprotein Ibα (clone: Xia.B2), and a DyLight 488-conjugated rat antibody against mouse CD42c (GPIbβ) were from Emfret Analytics (Eibelstadt, Germany). Tissue-Tek optimal cutting temperature compound was purchased from Thomas Scientific (Swedesboro, NJ). Vectashield Antifade mounting medium containing DAPI was obtained from Vector Laboratories (Burlingame, CA). A QuikChange Multi Site-Directed Mutagenesis kit was purchased from Agilent Technologies (Santa Clara, CA). 2-iodo-N-phenylacetamide (IPA) and ^{13}C-IPA were obtained from Cambridge Isotopes. Eptifibatide (Integrilin) was from Schering Plough (Kenilworth, NJ). Control IgG and rabbit polyclonal anti-PDI antibodies were labeled with Alexa Fluor 488 (Invitrogen) in parallel according to the manufacturer's instructions. The molar ratio of Alexa Fluor to IgG or antibodies, determined spectrophotometrically, was 3.5.

Isolation of platelets and neutrophils. Mouse and human platelets were prepared as previously described.[2] Washed platelets were suspended in HEPES-Tyrode buffer (20 mM HEPES, pH 7.4, 136 mM NaCl, 2.7 mM KCl, 12 mM $NaHCO_3$, 2 mM $MgCl_2$, and 5.5 mM glucose) and adjusted to a density of 3 x 10^8 cells/ml. Human blood and mouse bone marrow neutrophils were isolated as described previously.[3] The concentration of neutrophils was adjusted to 1 x 10^7 cells/ml in RPMI1640 media. The present study was

approved by the Institutional Review Board of the University of Illinois at Chicago. All healthy donors provided written informed consent before inclusion in the study.

Recombinant proteins. Recombinant human wild-type PDI (wtPDI) and its activity-null mutant (dmPDI in which two CysGlyHisCys sequences are mutated to SGHS) in a pET-15b vector carrying an N-terminal His tag (Novagen) were expressed in Clearcoil BL21 (DE3, Lucigen) to eliminate endotoxin.[4] The constructs of four different PDI domains (a, b, b'x, and a') were kindly provided from Robert Flaumenhaft (Beth Israel Deaconess Medical Center, Boston, MA) and expressed in the same manner. All proteins were purified using Ni^{2+}-affinity chromatography.

Purification of Anfibatide. Anfibatide, a specific antagonist of GPIbα, was purified from the snake venom of *Agkistrodon acutus* using ion exchange and gel filtration chromatography as described previously.[5] Purified Anfibatide was a heterodimeric protein of 29 kDa that is composed of α (15-kDa) and β (14-kDa) subunits as analyzed by SDS-PAGE electrophoresis.[5]

Platelet agglutination and aggregation assay. Washed mouse and human platelets in HEPES-Tyrode buffer (20 mM HEPES, pH 7.4, 136 mM NaCl, 2.7 mM KCl, 12 mM $NaHCO_3$, 2 mM $MgCl_2$, and 5.5 mM glucose) were incubated with 10 μg/ml vWF and 10 μg/ml botrocetin, and 5 μg/ml vWF and 0.3 mg/ml ristocetin, respectively. Platelets were pretreated with 10 μg/ml mouse IgG1 or a blocking anti-PDI antibody (BD34), and/or with 0.2 μg/ml BSA or Anfibatide for 30 minutes at 37°C. In some experiments, PDI-null

platelets were pretreated with 50 μg/ml wtPDI or dmPDI for 30 minutes at 37°C. In another experiment, platelets were pretreated with or without 10 μg/ml eptifibatide, different concentrations of Anfibatide, or 50 μM rutin, followed by incubation with vWF and either botrocetin or ristocetin. For aggregation assays, WT or hIL4R/GPIbα platelets in HEPES-Tyrode buffer were pretreated with or without 10 μg/ml eptifibatide and then stimulated with 0.025 U/ml thrombin. Platelet agglutination and aggregation were measured in a 4-channel platelet lumi-aggregometer (Chronolog Corp, Havertown, PA) at 37°C with stirring at 1,000 rpm.

Flow cytometry. Human or mouse platelets were treated with different doses (0.01, 0.025, 0.05 U/ml) of thrombin for 5 minutes at 37°C, followed by incubation with 50 μM PPACK. Cells were then incubated with PE- or Alexa Fluor 488-conjugated control IgG or antibodies against P-selectin, PDI or activated αIIbβ3 integrin. In some experiments, platelets were incubated with rat isotype control IgG or anti-GPIbα antibodies and then with Alexa Fluor 488 anti-rat IgG. Cells were analyzed by flow cytometric analysis (Cyan ADP, Beckman Coulter).

vWF binding assay. Mouse platelets were incubated with 10 μg/ml vWF in the presence or absence of 10 μg/ml botrocetin. To prevent the metalloprotease-mediated shedding of GPIbα and binding of vWF to αIIbβ3 integrin and P-selectin,[6-9] platelets were incubated with 10 mM EDTA prior to botrocetin stimulation. In some experiments, WT and PDI-null platelets were pretreated with 50 μg/ml wtPDI or dmPDI. In other experiments, mouse platelets were pretreated with vehicle or 10 μg/ml eptifibatide, 10 μg/ml control IgG, a

blocking anti-PDI antibody (BD34), or an anti-P-selectin antibody (RB40.34), and/or 0.2 μg/ml BSA or Anfibatide for 30 minutes at 37°C. After washing with HEPES-Tyrode buffer, platelets were incubated with 10 μg/ml vWF in the presence or absence of 10 μg/ml botrocetin for 10 minutes. In another experiment, WT or hIL4R/GPIbα platelets were used. Cells were then fixed with 1% paraformaldehyde, centrifuged at 800*g* for 2 minutes and resuspended in HEPES-Tyrode buffer. Cells were incubated with FITC-conjugated control IgG or rabbit anti-vWF antibodies for 30 minutes. Cells were analyzed by flow cytometric analysis (Cyan ADP, Beckman Coulter).

αMβ2 binding assay. Mouse or human platelets were pretreated with vehicle or 10 μg/ml eptifibatide, 10 μg/ml control IgG, a blocking anti-PDI antibody (BD34), or an anti-P-selectin antibody (RB40.34), and/or 0.2 μg/ml BSA or Anfibatide for 30 minutes at 37°C. After washing with HEPES-Tyrode buffer, platelets were incubated with recombinant human αMβ2, 10 μg/ml, in the presence or absence of 0.5 mM $MnCl_2$ for 30 minutes at 37°C. In some experiments, WT or PDI-null platelets were pretreated with or without 50 μg/ml wtPDI or dmPDI and then incubated with 10 μg/ml recombinant human αMβ2 in the presence or absence of 0.5 mM $MnCl_2$ for 30 minutes at 37°C. In another experiment, hIL4R/GPIbα platelets were incubated with αMβ2 in the presence or absence of 0.5 mM $MnCl_2$ and 50 μg/ml wtPDI for 30 minutes at 37°C. After washing out unbound αMβ2, platelets were incubated with 5 μg/ml FITC-conjugated control IgG or goat anti-human β2 antibodies, followed by flow cytometric analysis.

Surface plasmon resonance. The interaction of platelet surface PDI with GPIbα was

investigated by using surface plasmon resonance with Biacore T200. The extracellular domain of recombinant GPIbα (0.5 mg/ml in 10 mM sodium acetate buffer, pH 4.0) was immobilized onto a CM5 chip (Series S, Sensor Chip CM5, GE Healthcare) according to the manufacturer's instructions. Various concentrations of wtPDI or dmPDI (0.26 to 18 μM) or soluble αMβ2 (0.03 to 21 μM) in running buffer (10 mM HEPES, pH 7.5 including 150 mM NaCl, 0.05% Tween-20, 1 mM $MgCl_2$, 0.5 mM $MnCl_2$, and 1 mM dithiothreitol) were infused over the reference and integrin-immobilized surfaces at a flow rate of 15 μl/minute for 180 seconds, followed by a dissociation phase of 120 seconds. Specific binding between two proteins was calculated by subtracting the reference sensorgram from the sample. Data were analyzed with a software (Biacore T200 version 1.0, GE Healthcare).

Immunoprecipitation. Mouse platelets, 500 μl of 6 x 10^8 cells/ml, were stimulated with or without thrombin (0.025 U/ml) for 5 minutes at 37°C. The reaction was quenched with 50 μM PPACK. Platelets were then incubated with 100 μM SSB for 20 minutes at 37°C and then with 20 mM Tris-HCl, pH 7.4, to quench the reaction. After washing three times, platelets were lysed with ice-cold lysis buffer (20 mM TBS, pH 7.4, containing 1% Triton X-100, 0.1% SDS, 2 mM EDTA, 2 mM Na_3VO_4, protease inhibitor cocktail, and 2 mM phenylmethylsulfonyl fluoride), followed by incubation with control IgG or anti-PDI antibodies for 1 hour at room temperature and then with protein A/G beads for overnight at 4°C. The bound fractions were immunoblotted with indicated antibodies. The blots were stripped and re-probed with peroxidase-conjugated avidin. The band density was measured by densitometry using Scion Image (v4.0).

PDI binding assay. Platelets isolated from WT and hIL4R/GPIbα Tg mice were pretreated with 50 μg/ml His-tagged wtPDI or dmPDI for 30 minutes at 37°C. Platelets were then stimulated with or without 0.025 U/ml thrombin for 5 minutes at 37°C. The reaction was quenched with 50 μM PPACK. Cells were then incubated with Alexa Fluor 488-conjugated anti-His antibodies, followed by flow cytometric analysis.

ELISA. Recombinant GST-tagged GPIbα, 1 μg/ml, was immobilized on a well of a 96 well plate. After blocking with 1% BSA, different concentrations of wt and dmPDI, and its domain fragments (1 nM to 10 μM) in 20 mM HEPES buffer, pH 7.4, containing 1 mM glutathione were added to the well and incubated for 1 hour at room temperature. Then, anti-His antibodies, 1 μg/ml, were incubated for 1 hour at room temperature, followed by incubation with HRP-conjugated anti-mouse IgG antibodies. After the addition of 3,3',5,5'-tetramethylbenzidine (Pierce), the reaction was stopped with 1 N HCl. The signal was measured at 450 nm using a microplate reader (PHERAstar, BMG Labtec, Germany). Values obtained from BSA-coated surfaces were subtracted as a negative control. Data are shown as mean ± S.D. from 3-4 independent experiments.

Modeling of GPIbα-PDI binding. Coordinates of X-ray models of human GPIbα (protein data bank (PDB: 3P72)[10] and reduced (PDB: 4EKZ) and oxidized forms (PDB: 4EL1)[11] of human PDI were downloaded from the PDB. All molecular modeling studies were performed in Molecular Operating Environment (MOE).[12] The docking was unbiased and did not contain any pharmacophore requirements. The proteins were subjected to the

"structure preparation" procedure. Hydrogen atoms were added using the Protonate 3D algorithm. The energy of the resulting structure was minimized utilizing AMBER12EHT forcefield.[13] A short peptide found in GPIbα was removed. The proteins were minimized until the root mean square gradient was less than 0.001 kcal/mol/Å^2. The MOE module "Dock" for protein-protein docking was used to dock GPIbα to PDI using the default parameters and settings. Docking was performed using the "Rigid Body" refinement algorithm and "GBVI/WSA dG" function for rescoring of the resulting poses. A total of 100 poses were stored after the refinement step. The docking poses where the missing C-terminal of GPIbα was covered by PDI were discarded, and only those poses that did not have overlap with the missing C-terminal portion of GPIbα were considered for further analysis.

Free thiol labeling. GPIbα (50 nM) was incubated with either wtPDI or dmPDI (100 nM) for 10 minutes at 37°C, followed by incubation with 100 μM MPB for 30 minutes at 37°C in the presence of a mixture of GSH:GSSG (0:0, 1:0.33, or 1:0.05 mM). After quenching the reaction with 1 mM GSH, proteins were electrophoresed under reduced conditions and blotted with peroxidase-conjugated avidin or antibodies against GPIbα or PDI.

Mass spectrometry. The active site disulfide bond of PDI was reduced with 10 mM dithiothreitol for 30 minutes at room temperature, and the reducing agent was removed by a spin desalting column. Recombinant human GPIbα (His17-Leu505), 1.8 μM, was incubated without or with a 2- or 10-fold molar excess of wtPDI or dmPDI for 30 minutes at room temperature. Unpaired Cys thiols in GPIbα were alkylated with 5 mM 2-iodo-N-

phenylacetamide (^{12}C-IPA labeling free thiol groups of Cys residues forming allosteric disulfide bonds) for 1 hour at room temperature. The proteins were separated on SDS-PAGE and stained with SYPRO Ruby. The GPIbα band was excised, destained, dried and incubated with 40 mM dithiothreitol. The fully reduced GPIbα was alkylated for 1 hour at 25 °C with 5 mM ^{13}C-labeled IPA (^{13}C-IPA) where all 6 carbon atoms of the phenyl ring have a mass of 13. GPIbα was digested with 12.5 µg/ml trypsin in 25 mM NH_4CO_2 overnight at room temperature. Peptides were eluted from the slices with 5% formic acid and 50% acetonitrile, dried and reconstituted in 12 µl of 0.1% formic acid. Using a Thermo Fisher Scientific Ultimate 3000, peptides (3 µl) were injected and resolved on a 35 cm x 75 µm C18 reverse phase analytical column with integrated emitter over a gradient from 2% acetonitrile to 35% acetonitrile over 22 minutes with a flow rate of 200 nl/minute. The peptides were ionized by electrospray ionization at +2.0 kV. Tandem mass spectrometry analysis was carried out on a Q-Exactive Plus mass spectrometer (Thermo Fisher Scientific) using CID fragmentation. The data-dependent acquisition method acquired MS/MS spectra on the top 5 most abundant ions at any one point during the gradient. The data produced were searched using Mascot (Matrix Science) against UniProt database. Search parameters were as follows: precursor tolerance of 6 ppm and product ion tolerances of ± 0.4 Da. Cys-^{12}C-IPA, Cys-^{13}C-IPA, oxidized Met, pyro-Glu pyro-Gln were selected as variable modifications with full tryptic cleavage of up to three missed cleavages. To calculate ion abundance of peptides, extracted ion chromatograms were generated using the XCalibur Qual Browser software (v2.1.0; Thermo Scientific). The area was calculated using the automated peak detection function built into the software. The fraction of reduced disulfide bond was measured from the relative ion

abundance of peptides containing ^{12}C-IPA and ^{13}C-IPA. The ratio of ^{12}C-IPA to ^{13}C-IPA labeling of the Cys-containing peptides represented the fraction of the reduced disulfide bonds in GPIbα.

Chinese hamster ovary (CHO) cell transfection. The cDNAs of human wt or mutant (Cys4Ser or Cys209Ser) GPIbα, GPIbβ or GPIX were cloned into the pcDNA3.1 expression vector as described previously.[14] Site-directed mutagenesis for a Cys-to-Ser point mutation at the position of Cys4 or Cys209 was performed using QuikChange Multi Site-Directed Mutagenesis kit with the following primers: For the Cys4Ser mutation, a forward primer as 5'-CCCCCACCCCATCTCCGAGGTCTCCAA-3', and a reverse primer as 5'-CTTTGGAGACCTCGGAGATGGGGTGGG-3'. For the Cys209Ser mutation, a forward primer as 5'-GGGAACCCCTGGTTATCTAACTGTGAGATCCTC-3', and a reverse primer as 5'-GAGGATCTCACAGTTAGATAACCAGGGGTTCCC-3'. The cDNAs were co-transfected into CHO cells using Lipofectamine 2000 according to the manufacturer's instructions. Cells were harvested with 1 mM EDTA after 60 hours of transfection. CHO cells expressing wt or mutant GPIb-IX (5×10^5) were suspended in HEPES-Tyrode buffer. The expression of cell surface GPIbα was detected by flow cytometer using three different anti-GPIbα antibodies: HIP1 that recognizes the N-terminal vWF-binding domain, SZ2 that binds to the anionic sulfated tyrosine region, and MM2/174 that recognizes the elastase-resistant part of GPIbα.[15-17] In some experiments, cells were incubated with 35 μg/ml vWF and 2 mg/ml ristocetin in an aggregometer at 37°C with stirring at 200g for 10 minutes. The unbound vWF was washed out by centrifugation at 800g for 5 minutes. Cells were treated with isotype control IgG or anti-

GPIbα antibodies (MM2/174), followed by incubation with Alexa Fluor 647-conjugated anti-mouse IgG antibodies. Then, cells were incubated with FITC-conjugated control IgG or anti-vWF antibodies.

In vitro **heterotypic platelet-neutrophil aggregation**. Platelet-neutrophil aggregation assays were performed as previously described.[2] Platelets (2×10^7) and neutrophils (1×10^6) isolated from WT and PDI CKO mice were labeled with DyLight 488-conjugated anti-CD42c and Alexa Fluor 647-conjugated anti-Ly-6G antibodies, respectively. Human neutrophils and platelets were labeled with Alexa Fluor 488-conjugated anti-CD41 and FITC-conjugated anti-L-selectin antibodies, respectively. Neutrophils were stimulated with 20 ng/ml TNF-α for 5 minutes. Platelets were pretreated with or without control IgG or a blocking anti-PDI antibody (10 μg/ml), BSA or Anfibatide (0.2 μg/ml), or both inhibitors for 30 minutes at room temperature and then activated with 0.025 U/ml thrombin for 5 minutes at 37°C, followed by incubation with 50 μM PPACK. Activated platelets were mixed with stimulated neutrophils under a stirring condition of 1,000 rpm in an aggregometer. After a 5-minute incubation, cells were fixed and analyzed by flow cytometry. Cell-cell aggregation was assessed by the number of cell-cell aggregates in the R3 gate and the mean fluorescence intensities (MFI) of anti-CD42c antibodies (Heterotypic interaction) in the R1 gate. Data were presented as the percentage of the number of cell aggregates (for cell-cell aggregates) or the MFI value (for heterotypic interaction) normalized to a control group (WT platelets/neutrophils or control IgG-treated cells). In some experiments, antibody-labeled platelets and neutrophils were mixed under stirring and cytospinned at 200g for 10 minutes. Fluorescence images were captured with

a Nikon microscope (ECLIPSE Ti, Melville, NY) equipped with a Plan Fluor ×40/1.30NA oil objective lens and recorded with a digital camera (CoolSNAP ES2) as described previously.[18] The data were analyzed using NIS-Elements (AR 3.2; Nikon).

Proximity ligation assay. WT control and PDI CKO mice were treated with intrascrotal injection of TNF-α, 500 ng. Three hours later, the cremaster muscle was removed and mounted on dental wax to retain the stretched conformation of the tissue. The muscle was washed with PBS and cryopreserved in optimal cutting temperature compound. The frozen blocks were cryosectioned and then mounted to slides. The thawed slides were rehydrated in PBS for 10 minutes at room temperature and blocked with the blocking solution provided by Duolink® In Situ Red Proximity Ligation Assay kit at 37°C for 1 hour, followed by incubation with nonimmune goat IgG and rabbit IgG, or goat anti-PDI and rabbit anti-GPIbα antibodies (1 μg/ml) at room temperature for 1 hour. Duolink proximity ligation assay was performed according to the manufacturer's instructions. After washing, platelets and neutrophils were labeled with DyLight 488-conjugated anti-CD42c and Alexa Fluor 647-conjugated anti-Ly-6G antibodies (10 μg/ml), respectively. The slides were mounted with Vectashield containing DAPI. Images were acquired on a Zeiss LSM 880 confocal microscope (Carl Zeiss AG, Germany) equipped with a Plan Apochromatic 63x/1.4 oil immersion objective. The number of platelets and the PLA signal (i.e. single dots) were counted using a Zen 2 (blue edition) software (Carl Zeiss AG, Germany). Twenty vessels in 6 different sections were acquired from three different mice per group. The number of PLA puncta was normalized to the number of platelets in each vessel.

Ischemia/reperfusion-induced stroke. Both male and female C57BL/6 mice, WT, platelet-specific PDI CKO mice (22-25g, 7-10 weeks old) were anesthetized 2% isoflurane in oxygen mixture and treated by ip injection of buprenorphine (30 ng/g BW, i.p.). The body temperature was maintained at 37°C throughout surgery using a heating blanket. The left common carotid artery was exposed, followed by dissection of the external carotid artery and isolation of the internal carotid artery. A left middle cerebral artery was occluded with a monofilament (0.15 mm in diameter, the tip diameter is 0.22-0.25 mm, 5-0 DERMALON, Syneture) for 1 hour. A successful occlusion was indicated by a decrease in the regional cerebral blood flow to <20% of the baseline using a laser Doppler perfusion monitoring system (PF5010, Perimed AB, Ardmore, PA). The filament was then removed, and blood flow was restored to the baseline. BSA or Anfibatide (5 or 25 ng/g BW in 100 µl saline) was intravenously infused into mice after 1-hour occlusion. The experiments were performed in a single-blind manner. After re-injection of buprenorphine (25 ng/g BW i.p.), mice were subjected to 23 hours of reperfusion. Neurological function was then assessed using the Bederson score[19] and Wire suspension test (grip test).[20] For measuring Bederson score, neurological deficits were scored according to the following system: 0, no observable deficit; 1, forelimb flexion; 2, forelimb flexion and decreased resistance to lateral push; 3, forelimb flexion, decreased resistance to lateral push, and circle to paretic side. For the wire suspension test of grip strength and endurance, the mouse placed on a horizontal string (0.5 mm thick, 50 cm in length, 40 cm above a tabletop). The mouse was assessed according to the following system: 0, falls off; 1, hung onto the string with two forepaws; 2, in addition to 1, attempted to climb onto string; 3, hung onto the string with two forepaws and one or both hindpaws; 4, hung onto the string

with four paws with tail wrapped around the string; 5, escape to the edge of the string. After the assessment, mice were sacrificed, and brains were taken out. The 2-mm brain slices were stained with 2% 2,3,5-triphenyltetrazolium chloride solution (Sigma-Aldrich) for 10 minutes at 37°C, followed by fixation with 4% paraformaldehyde. Sections were scanned, and the infarct volumes were measured using Image J.

REFERENCES

1. Andrews RK, Booth WJ, Gorman JJ, Castaldi PA and Berndt MC. Purification of botrocetin from Bothrops jararaca venom. Analysis of the botrocetin-mediated interaction between von Willebrand factor and the human platelet membrane glycoprotein Ib-IX complex. *Biochemistry*. 1989;28:8317-8326.

2. Kim K, Li J, Tseng A, Andrews RK and Cho J. NOX2 is critical for heterotypic neutrophil-platelet interactions during vascular inflammation. *Blood*. 2015;126:1952-1964.

3. Hahm E, Li J, Kim K, Huh S, Rogelj S and Cho J. Extracellular protein disulfide isomerase regulates ligand-binding activity of alphaMbeta2 integrin and neutrophil recruitment during vascular inflammation. *Blood*. 2013;121:3789-3800.

4. Planesse C, Nativel B, Iwema T, Gasque P, Robert-Da Silva C and Viranaicken W. Recombinant human HSP60 produced in ClearColi BL21(DE3) does not activate the NFkappaB pathway. *Cytokine*. 2015;73:190-195.

5. Cheng X, Qian Y, Liu Q, Li BX, Zhang M and Liu J. Purification, characterization, and cDNA cloning of a new fibrinogenlytic venom protein, Agkisacutacin, from Agkistrodon acutus venom. *Biochem Biophys Res Commun*. 1999;265:530-535.

6. Gardiner EE, Karunakaran D, Shen Y, Arthur JF, Andrews RK and Berndt MC.

Controlled shedding of platelet glycoprotein (GP)VI and GPIb-IX-V by ADAM family metalloproteinases. *J Thromb Haemost*. 2007;5:1530-1537.

7. Deng W, Xu Y, Chen W, Paul DS, Syed AK, Dragovich MA, Liang X, Zakas P, Berndt MC, Di Paola J, Ware J, Lanza F, Doering CB, Bergmeier W, Zhang XF and Li R. Platelet clearance via shear-induced unfolding of a membrane mechanoreceptor. *Nat Commun*. 2016;7:12863.

8. Padilla A, Moake JL, Bernardo A, Ball C, Wang Y, Arya M, Nolasco L, Turner N, Berndt MC, Anvari B, Lopez JA and Dong JF. P-selectin anchors newly released ultralarge von Willebrand factor multimers to the endothelial cell surface. *Blood*. 2004;103:2150-2156.

9. Weisel JW, Nagaswami C, Vilaire G and Bennett JS. Examination of the platelet membrane glycoprotein IIb-IIIa complex and its interaction with fibrinogen and other ligands by electron microscopy. *J Biol Chem*. 1992;267:16637-16643.

10. McEwan PA, Andrews RK and Emsley J. Glycoprotein Ibalpha inhibitor complex structure reveals a combined steric and allosteric mechanism of von Willebrand factor antagonism. *Blood*. 2009;114:4883-4885.

11. Wang C, Li W, Ren J, Fang J, Ke H, Gong W, Feng W and Wang CC. Structural insights into the redox-regulated dynamic conformations of human protein disulfide isomerase. *Antioxid Redox Signal*. 2013;19:36-45.

12. Molecular Operating Environment (MOE) CCGU, 1010 Sherbooke St. West, Suite #910, Montreal, QC, Canada, H3A 2R7, 2018.

13. Gerber PR and Muller K. MAB, a generally applicable molecular force field for structure modelling in medicinal chemistry. *J Comput Aided Mol Des*. 1995;9:251-268.

14. Dai K, Bodnar R, Berndt MC and Du X. A critical role for 14-3-3zeta protein in regulating the VWF binding function of platelet glycoprotein Ib-IX and its therapeutic implications. *Blood*. 2005;106:1975-1981.

15. Kuijpers RW, Ouwehand WH, Bleeker PM, Christie D and von dem Borne AE. Localization of the platelet-specific HPA-2 (Ko) alloantigens on the N-terminal globular fragment of platelet glycoprotein Ib alpha. *Blood*. 1992;79:283-288.

16. Simon DI, Chen Z, Xu H, Li CQ, Dong J, McIntire LV, Ballantyne CM, Zhang L, Furman MI, Berndt MC and Lopez JA. Platelet glycoprotein ibalpha is a counterreceptor for the leukocyte integrin Mac-1 (CD11b/CD18). *J Exp Med*. 2000;192:193-204.

17. Kunishima S, Matsushita T, Ito T, Kamiya T and Saito H. Novel nonsense mutation in the platelet glycoprotein Ibbeta gene associated with Bernard-Soulier syndrome. *Am J Hematol*. 2002;71:279-284.

18. Li J, Kim K, Hahm E, Molokie R, Hay N, Gordeuk VR, Du X and Cho J. Neutrophil AKT2 regulates heterotypic cell-cell interactions during vascular inflammation. *J Clin Invest*. 2014;124:1483-1496.

19. Bederson JB, Pitts LH, Tsuji M, Nishimura MC, Davis RL and Bartkowski H. Rat middle cerebral artery occlusion: evaluation of the model and development of a neurologic examination. *Stroke*. 1986;17:472-476.

20. Moran PM, Higgins LS, Cordell B and Moser PC. Age-related learning deficits in transgenic mice expressing the 751-amino acid isoform of human beta-amyloid precursor protein. *Proc Natl Acad Sci U S A.* 1995;92:5341-5345.

Supplemental Table S1. Allosteric disulfide bonds in platelet surface proteins.

Family	Receptor	Cysteine	Allosteric configuration	PDB ID*	References
β3 integrin	αIIb	Cys56-Cys65	-RHStaple	1TYE, 2VC2, 2VDK, 2VDL, 2VDM, 2VDN, 2VDO, 2VDP, 2VDQ, 2VDR, 3FCS, 3FCU, 3NID, 3NIF, 3NIG, 3T3M, 3T3P, 3ZDX, 3ZDY, 3ZDZ, 3ZE0, 3ZE1, 3ZE2, 4Z7N, 4Z7O, 4Z7Q, and 5HDB	[1], [2], [3], [4], [5], [6], [7]
		Cys107-Cys130	-RHStaple		
		Cys146-Cys167	-LHHook		
		Cys602-Cys608	-LHHook		
		Cys473-Cys484	-/+RHHook		
		Cys490-Cys545	-RHStaple		
		Cys674-Cys687	-RHStaple		
		Cys826-Cys890	-RHStaple		
	β3	Cys26-Cys49	-LHHook		
		Cys177-Cys184	-/+RHHook		
		Cys406-Cys433	-/+RHHook		
		Cys437-Cys457	-/+RHHook		
		Cys462-Cys471	-LHHook		
		Cys473-Cys503	-/+RHHook		
		Cys523-Cys544	-LHHook		
		Cys560-Cys583	-LHHook		
		Cys614-Cys635	-/+RHHook		
		Cys663-Cys687	-RHStaple		
	αv	Cys59-Cys67	-RHStaple	4G1M, 3IJE, 1L5G, 1M1X, 4MMX, 4MMY, 4MMZ, and 4O02	[8], [9], [10], [11], [12]
		Cys108-Cys128	-RHStaple		
		Cys142-Cys155	-/+RHHook		
		Cys478-Cys535	-LHHook,-RHStaple		
		Cys596-Cys602	-LHHook		
		Cys668-Cys681	-RHStaple		
		Cys822-Cys884	-RHStaple		
		Cys874-Cys879	-RHStaple		
	β3	Cys13-Cys435	-LHHook		
		Cys177-Cys184	-/+RHHook		
		Cys406-Cys433	-/+RHHook		
		Cys437-Cys457	-/+RHHook		
		Cys448-Cys460	-/+RHHook		

		Cys462-Cys471 Cys486-Cys501 Cys495-Cys506 Cys523-Cys544 Cys560-Cys583 Cys617-Cys631 Cys663-Cys687	-LHHook -LHHook -LHHook -LHHook,-RHStaple -LHHook -LHHook -RHStaple		
β1 integrin	α2	No allosteric configuration		1AOX	[13]
	α5	Cys58-Cys67 Cys115-Cys135 Cys487-Cys543	-RHStaple -RHStaple -RHStaple	3VI4, 4WJK, and 4WK2	[14], [15]
	β1	Cys7-Cys25 Cys15-Cys444 Cys28-Cys55	-LHHook -LHHook -LHHook		
	α6	No allosteric configuration		Not available	
GPIb-IX-V	GPIbα	Cys4-Cys17 Cys209-Cys248	-RHStaple -LHHook	1M0Z, 1M10, 1OOK, 1P9A, 1QYY, and 3P72	[16], [17], [18], [19]
	GPIbβ	Cys5-Cys14	-RHStaple	3REZ and 3RFE	[20]
		Cys68-Cys93	-LHHook		
	GPIX	No allosteric configuration		3REZ	[20]
	GPV	No allosteric configuration		Not available	
Toll-like receptors (TLR)	TLR1	Cys223-Cys230	-/+RHHook	1FYV and 2Z7X	[21, 22]
		Cys667-Cys686	-/+RHHook		
	TLR2	Cys10-Cys16 Cys295-Cys320 Cys517-Cys542	-RHStaple -LHHook -LHHook	2Z7X and 2Z80	[22]
	TLR4	Cys6-Cys17 Cys241-Cys266 Cys367-Cys368 Cys560-Cys586	-RHStaple -LHHook -RHStaple -LHHook	2Z62, 3UL7, 3UL8, 3UL9, and 4G8A	[23], [24], [25]
	TLR6	No allosteric configuration		4OM7	[26]
	TLR7	No allosteric configuration		Not available	
	TLR9	No allosteric configuration		Not available	
Thrombin receptors	PAR1	No allosteric configuration		Not available	
	PAR4	No allosteric configuration		Not available	

ADP receptors	P2Y1	No allosteric configuration		4XNV and 4XNW	[27]
	P2Y12	No allosteric configuration		4PXZ and 4PY0	[28]
Prostaglandin receptors	Thromboxane receptor A2	No allosteric configuration		1LBN	Theoretical model
	PGI2 receptor	No allosteric configuration		Not available	
	PGD2 receptor	No allosteric configuration		Not available	
	PGE2 receptor	No allosteric configuration		Not available	
Vasopressin receptor	V1a receptor	No allosteric configuration		1YTV	[29]
Adenosine receptor	A2a receptor	Cys74-Cys146 Cys77-Cys166	-LHHook -LHHook	3VG9 and 3VGA	[30]
Epinephrine receptor	β2-Adrenergic receptor	Cys184-Cys190	-LHHook	2RH1, 3NY8, 3NY9, 3NYA, 3P0G, 3PDS, 5D5A, 5D5B, and 5D6L	[31], [32], [33], [34], [35], [36]
Serotonin receptor	5-HT2A receptor	No allosteric configuration		Not available	
Dopamine receptor	D3	No allosteric configuration		3PBL	[37]
	D5	No allosteric configuration		Not available	
Chemokine receptor	CXCR1	No allosteric configuration		2LNL, 1ILP, and 1ILQ	[38]
	CXCR2	No allosteric configuration		5TYT	[39]
	CXCR4	Cys28-Cys274	-LHHook	3OE8 and 3OE9	[40]
	CCR1	No allosteric configuration		1Y5D	Theoretical model
	CCR3	No allosteric configuration		Not available	
	CCR4	No allosteric configuration		Not available	
Collagen receptor	GPVI	No allosteric configuration		2GI7	[41]
	CLEC-2	No allosteric configuration		3WSR and 2C6U	[42], [43]
	CD40	Cys6-Cys17 Cys85-Cys99 Cys91-Cys96 Cys105-Cys123 Cys147-Cys166	-LHHook -LHHook -LHHook -LHHook -LHHook	5DMI, 5DMJ, and 5IHL	[44]
	CD40L	No allosteric configuration		3QD6	[45]

	P-selectin	No allosteric configuration		1FSB, 1G1Q, 1G1R, and 1G1S	[46], [47]
Junctional adhesion molecules	JAM-C	No allosteric configuration		Not available	
Intercellular adhesion molecules	ICAM-2	No allosteric configuration		1ZXQ	[48]
Complement receptor	C1qRp	No allosteric configuration		Not available	
Anaphylatoxin receptors	C3aR	No allosteric configuration		Not available	
	C5aR	No allosteric configuration		5O9H	[49]
Major histocompatibility complex class	MHC-1	Cys203-Cys259	-LHHook	3RWC, 3RWD, 3RWE, 3RWF, 3RWG, 3RWH, 3RWI, and 3RWJ	[50]
Sialic acid-binding receptors	Siglec-7	No allosteric configuration		1NKO, 1O7S, 1O7V, 2DF3, 2G5R, and 2HRL	[51],[52],[53],[54]
	Siglec-9	No allosteric configuration		Not available	
	Siglec-11	No allosteric configuration		Not available	
	CD36	No allosteric configuration		5LGD	[55]
Nucleotide-binding oligomerization domain-containing protein	NOD2	No allosteric configuration		5IRL, 5IRM, and 5IRN	[56]
Scavenger receptor	SRB1	No allosteric configuration		5KTF and 3R69	[57,58]
	PECAM-1	Cys30-Cys82 Cys125-Cys179	-LHHook -LHHook	2KY5, 5C14, and 5GNI	[59],[60],[61]
Insulin receptor	INSR	Cys8-Cys26	-LHHook	1GAG, 1I44, 1IR3,	[62],[63],[64],[65],[66],[67],

				1IRK, 1P14, 1RQQ, 2AUH, 2B4S, 2HR7, 2MFR, 2Z8C, 3BU3, 3BU5, 3BU6, 3EKK, 3EKN, 3ETA, 3W11, 4XLV, 4XSS, 4XST, 4ZXB, 5E1S, 5HHW, 5J3H, 5KQV, 5U1M, 3W12, 3W13, 4IBM, and 4OGA	[68,69,70,71,72,73,74,75,76,77,78,79,80,81,82,76,83,76,84,85]
Leptin receptor	LEPR	Cys415-Cys426 Cys467-Cys477	-RHStaple -RHStaple	3V6O	[86]
Platelet-activating factor receptor	PAF-R	No allosteric configuration		2B0X	Theoretical model
TREM-like transcript-1	TLT-1	No allosteric configuration		2FRG	[87]
Tyrosine-protein kinase receptor	Tie-1	No allosteric configuration		5N06	[88]
SLAM family member	CD84 (SLAMF5)	No allosteric configuration		2PKD	[89]
	CD150 (SLAMF1)	No allosteric configuration		1M27	
Platelet-derived growth factor receptor	PDGFR1	No allosteric configuration		1GQ5, 1H9O, 1LWP, 1SHA, 2L6W, 2PLD, 2PLE, and 3MJG	[90,91,92,93,94,95]
	PDGFR2	No allosteric configuration		1GQ5 and 5GRN	[90]

*: Protein Data Bank Identifier

References

1. Xiao T, Takagi J, Coller BS, Wang JH and Springer TA. Structural basis for allostery in integrins and binding to fibrinogen-mimetic therapeutics. *Nature*. 2004;432:59-67.
2. Springer TA, Zhu J and Xiao T. Structural basis for distinctive recognition of fibrinogen gammaC peptide by the platelet integrin alphaIIbbeta3. *J Cell Biol*. 2008;182:791-800.
3. Zhu J, Luo BH, Xiao T, Zhang C, Nishida N and Springer TA. Structure of a complete integrin ectodomain in a physiologic resting state and activation and deactivation by applied forces. *Mol Cell*. 2008;32:849-861.
4. Zhu J, Zhu J, Negri A, Provasi D, Filizola M, Coller BS and Springer TA. Closed headpiece of integrin alphaIIbbeta3 and its complex with an alphaIIbbeta3-specific antagonist that does not induce opening. *Blood*. 2010;116:5050-5059.
5. Zhu J, Choi WS, McCoy JG, Negri A, Zhu J, Naini S, Li J, Shen M, Huang W, Bougie D, Rasmussen M, Aster R, Thomas CJ, Filizola M, Springer TA and Coller BS. Structure-guided design of a high-affinity platelet integrin alphaIIbbeta3 receptor antagonist that disrupts Mg(2)(+) binding to the MIDAS. *Sci Transl Med*. 2012;4:125ra32.
6. Zhu J, Zhu J and Springer TA. Complete integrin headpiece opening in eight steps. *J Cell Biol*. 2013;201:1053-1068.
7. Lin FY, Zhu J, Eng ET, Hudson NE and Springer TA. beta-Subunit Binding Is Sufficient for Ligands to Open the Integrin alphaIIbbeta3 Headpiece. *J Biol Chem*. 2016;291:4537-4546.
8. Dong X, Mi LZ, Zhu J, Wang W, Hu P, Luo BH and Springer TA. alpha(V)beta(3) integrin crystal structures and their functional implications. *Biochemistry*. 2012;51:8814-8828.
9. Xiong JP, Stehle T, Zhang R, Joachimiak A, Frech M, Goodman SL and Arnaout MA. Crystal structure of the extracellular segment of integrin alpha Vbeta3 in complex with an Arg-Gly-Asp ligand. *Science*. 2002;296:151-155.
10. Van Agthoven JF, Xiong JP, Alonso JL, Rui X, Adair BD, Goodman SL and Arnaout MA. Structural basis for pure antagonism of integrin alphaVbeta3 by a high-affinity form of fibronectin. *Nat Struct Mol Biol*. 2014;21:383-388.
11. Mahalingam B, Van Agthoven JF, Xiong JP, Alonso JL, Adair BD, Rui X, Anand S, Mehrbod M, Mofrad MR, Burger C, Goodman SL and Arnaout MA. Atomic basis for the species-specific inhibition of alphaV integrins by monoclonal antibody 17E6 is revealed by the crystal structure of alphaVbeta3 ectodomain-17E6 Fab complex. *J Biol Chem*. 2014;289:13801-13809.
12. Dong X, Zhao B, Iacob RE, Zhu J, Koksal AC, Lu C, Engen JR and Springer TA. Force interacts with macromolecular structure in activation of TGF-beta. *Nature*. 2017;542:55-59.
13. Emsley J, King SL, Bergelson JM and Liddington RC. Crystal structure of the I domain from integrin alpha2beta1. *J Biol Chem*. 1997;272:28512-28517.
14. Nagae M, Re S, Mihara E, Nogi T, Sugita Y and Takagi J. Crystal structure of alpha5beta1 integrin ectodomain: atomic details of the fibronectin receptor. *J Cell Biol*. 2012;197:131-140.
15. Xia W and Springer TA. Metal ion and ligand binding of integrin alpha5beta1. *Proc. Natl. Acad. Sci. U.S.A.* 2014;111:17863-17868.

16. Huizinga EG, Tsuji S, Romijn RA, Schiphorst ME, de Groot PG, Sixma JJ and Gros P. Structures of glycoprotein Ibalpha and its complex with von Willebrand factor A1 domain. *Science*. 2002;297:1176-1179.
17. Celikel R, McClintock RA, Roberts JR, Mendolicchio GL, Ware J, Varughese KI and Ruggeri ZM. Modulation of alpha-thrombin function by distinct interactions with platelet glycoprotein Ibalpha. *Science*. 2003;301:218-221.
18. Varughese KI, Ruggeri ZM and Celikel R. Platinum-induced space-group transformation in crystals of the platelet glycoprotein Ib alpha N-terminal domain. *Acta Crystallogr D Biol Crystallogr*. 2004;60:405-411.
19. McEwan PA, Andrews RK and Emsley J. Glycoprotein Ibalpha inhibitor complex structure reveals a combined steric and allosteric mechanism of von Willebrand factor antagonism. *Blood*. 2009;114:4883-4885.
20. McEwan PA, Yang W, Carr KH, Mo X, Zheng X, Li R and Emsley J. Quaternary organization of GPIb-IX complex and insights into Bernard-Soulier syndrome revealed by the structures of GPIbbeta and a GPIbbeta/GPIX chimera. *Blood*. 2011;118:5292-5301.
21. Xu Y, Tao X, Shen B, Horng T, Medzhitov R, Manley JL and Tong L. Structural basis for signal transduction by the Toll/interleukin-1 receptor domains. *Nature*. 2000;408:111-115.
22. Jin MS, Kim SE, Heo JY, Lee ME, Kim HM, Paik SG, Lee H and Lee JO. Crystal structure of the TLR1-TLR2 heterodimer induced by binding of a tri-acylated lipopeptide. *Cell*. 2007;130:1071-1082.
23. Kim HM, Park BS, Kim JI, Kim SE, Lee J, Oh SC, Enkhbayar P, Matsushima N, Lee H, Yoo OJ and Lee JO. Crystal structure of the TLR4-MD-2 complex with bound endotoxin antagonist Eritoran. *Cell*. 2007;130:906-917.
24. Han J, Kim HJ, Lee SC, Hong S, Park K, Jeon YH, Kim D, Cheong HK and Kim HS. Structure-based rational design of a Toll-like receptor 4 (TLR4) decoy receptor with high binding affinity for a target protein. *PloS one*. 2012;7:e30929.
25. Ohto U, Yamakawa N, Akashi-Takamura S, Miyake K and Shimizu T. Structural analyses of human Toll-like receptor 4 polymorphisms D299G and T399I. *J Biol Chem*. 2012;287:40611-40617.
26. Jang TH and Park HH. Crystal structure of TIR domain of TLR6 reveals novel dimeric interface of TIR-TIR interaction for toll-like receptor signaling pathway. *J Mol Biol*. 2014;426:3305-3313.
27. Zhang D, Gao ZG, Zhang K, Kiselev E, Crane S, Wang J, Paoletta S, Yi C, Ma L, Zhang W, Han GW, Liu H, Cherezov V, Katritch V, Jiang H, Stevens RC, Jacobson KA, Zhao Q and Wu B. Two disparate ligand-binding sites in the human P2Y1 receptor. *Nature*. 2015;520:317-321.
28. Zhang J, Zhang K, Gao ZG, Paoletta S, Zhang D, Han GW, Li T, Ma L, Zhang W, Muller CE, Yang H, Jiang H, Cherezov V, Katritch V, Jacobson KA, Stevens RC, Wu B and Zhao Q. Agonist-bound structure of the human P2Y12 receptor. *Nature*. 2014;509:119-122.
29. Adikesavan NV, Mahmood SS, Stanley N, Xu Z, Wu N, Thibonnier M and Shoham M. A C-terminal segment of the V1R vasopressin receptor is unstructured in the crystal structure of its chimera with the maltose-binding protein. *Acta Crystallogr Sect F Struct Biol Cryst Commun.* 2005;61:341-345.
30. Hino T, Arakawa T, Iwanari H, Yurugi-Kobayashi T, Ikeda-Suno C, Nakada-Nakura Y, Kusano-Arai O, Weyand S,

Shimamura T, Nomura N, Cameron AD, Kobayashi T, Hamakubo T, Iwata S and Murata T. G-protein-coupled receptor inactivation by an allosteric inverse-agonist antibody. *Nature*. 2012;482:237-240.
31. Cherezov V, Rosenbaum DM, Hanson MA, Rasmussen SG, Thian FS, Kobilka TS, Choi HJ, Kuhn P, Weis WI, Kobilka BK and Stevens RC. High-resolution crystal structure of an engineered human beta2-adrenergic G protein-coupled receptor. *Science*. 2007;318:1258-1265.
32. Wacker D, Fenalti G, Brown MA, Katritch V, Abagyan R, Cherezov V and Stevens RC. Conserved binding mode of human beta2 adrenergic receptor inverse agonists and antagonist revealed by X-ray crystallography. *J Am Chem Soc*. 2010;132:11443-11445.
33. Rasmussen SG, Choi HJ, Fung JJ, Pardon E, Casarosa P, Chae PS, Devree BT, Rosenbaum DM, Thian FS, Kobilka TS, Schnapp A, Konetzki I, Sunahara RK, Gellman SH, Pautsch A, Steyaert J, Weis WI and Kobilka BK. Structure of a nanobody-stabilized active state of the beta(2) adrenoceptor. *Nature*. 2011;469:175-180.
34. Rosenbaum DM, Zhang C, Lyons JA, Holl R, Aragao D, Arlow DH, Rasmussen SG, Choi HJ, Devree BT, Sunahara RK, Chae PS, Gellman SH, Dror RO, Shaw DE, Weis WI, Caffrey M, Gmeiner P and Kobilka BK. Structure and function of an irreversible agonist-beta(2) adrenoceptor complex. *Nature*. 2011;469:236-240.
35. Huang CY, Olieric V, Ma P, Howe N, Vogeley L, Liu X, Warshamanage R, Weinert T, Panepucci E, Kobilka B, Diederichs K, Wang M and Caffrey M. In meso in situ serial X-ray crystallography of soluble and membrane proteins at cryogenic temperatures. *Acta Crystallogr D Struct Biol*. 2016;72:93-112.
36. Ma P, Weichert D, Aleksandrov LA, Jensen TJ, Riordan JR, Liu X, Kobilka BK and Caffrey M. The cubicon method for concentrating membrane proteins in the cubic mesophase. *Nat Protoc*. 2017;12:1745-1762.
37. Chien EY, Liu W, Zhao Q, Katritch V, Han GW, Hanson MA, Shi L, Newman AH, Javitch JA, Cherezov V and Stevens RC. Structure of the human dopamine D3 receptor in complex with a D2/D3 selective antagonist. *Science*. 2010;330:1091-1095.
38. Skelton NJ, Quan C, Reilly D and Lowman H. Structure of a CXC chemokine-receptor fragment in complex with interleukin-8. *Structure*. 1999;7:157-168.
39. Spellmon N, Holcomb J, Niu A, Choudhary V, Sun X, Zhang Y, Wan J, Doughan M, Hayden S, Hachem F, Brunzelle J, Li C and Yang Z. Structural basis of PDZ-mediated chemokine receptor CXCR2 scaffolding by guanine nucleotide exchange factor PDZ-RhoGEF. *Biochem Biophys Res Commun*. 2017;485:529-534.
40. Wu B, Chien EY, Mol CD, Fenalti G, Liu W, Katritch V, Abagyan R, Brooun A, Wells P, Bi FC, Hamel DJ, Kuhn P, Handel TM, Cherezov V and Stevens RC. Structures of the CXCR4 chemokine GPCR with small-molecule and cyclic peptide antagonists. *Science*. 2010;330:1066-1071.
41. Horii K, Kahn ML and Herr AB. Structural basis for platelet collagen responses by the immune-type receptor glycoprotein VI. *Blood*. 2006;108:936-942.
42. Nagae M, Morita-Matsumoto K, Kato M, Kaneko MK, Kato Y and Yamaguchi Y. A platform of C-type lectin-like

receptor CLEC-2 for binding O-glycosylated podoplanin and nonglycosylated rhodocytin. *Structure*. 2014;22:1711-1121.
43. Watson AA, Brown J, Harlos K, Eble JA, Walter TS and O'Callaghan CA. The crystal structure and mutational binding analysis of the extracellular domain of the platelet-activating receptor CLEC-2. *J Biol Chem*. 2007;282:3165-3172.
44. Yamniuk AP, Suri A, Krystek SR, Tamura J, Ramamurthy V, Kuhn R, Carroll K, Fleener C, Ryseck R, Cheng L, An Y, Drew P, Grant S, Suchard SJ, Nadler SG, Bryson JW and Sheriff S. Functional Antagonism of Human CD40 Achieved by Targeting a Unique Species-Specific Epitope. *J Mol Biol*. 2016;428:2860-2879.
45. An HJ, Kim YJ, Song DH, Park BS, Kim HM, Lee JD, Paik SG, Lee JO and Lee H. Crystallographic and mutational analysis of the CD40-CD154 complex and its implications for receptor activation. *J Biol Chem*. 2011;286:11226-11235.
46. Freedman SJ, Sanford DG, Bachovchin WW, Furie BC, Baleja JD and Furie B. Structure and function of the epidermal growth factor domain of P-selectin. *Biochemistry*. 1996;35:13733-13744.
47. Somers WS, Tang J, Shaw GD and Camphausen RT. Insights into the molecular basis of leukocyte tethering and rolling revealed by structures of P- and E-selectin bound to SLe(X) and PSGL-1. *Cell*. 2000;103:467-479.
48. Casasnovas JM, Springer TA, Liu JH, Harrison SC and Wang JH. Crystal structure of ICAM-2 reveals a distinctive integrin recognition surface. *Nature*. 1997;387:312-315.
49. Robertson N, Rappas M, Dore AS, Brown J, Bottegoni G, Koglin M, Cansfield J, Jazayeri A, Cooke RM and Marshall FH. Structure of the complement C5a receptor bound to the extra-helical antagonist NDT9513727. *Nature*. 2018;553:111-114.
50. Wu Y, Gao F, Liu J, Qi J, Gostick E, Price DA and Gao GF. Structural basis of diverse peptide accommodation by the rhesus macaque MHC class I molecule Mamu-B*17: insights into immune protection from simian immunodeficiency virus. *J Immunol*. 2011;187:6382-6392.
51. Dimasi N, Moretta A, Moretta L, Biassoni R and Mariuzza RA. Structure of the saccharide-binding domain of the human natural killer cell inhibitory receptor p75/AIRM1. *Acta Crystallogr D Biol Crystallogr*. 2004;60:401-403.
52. Alphey MS, Attrill H, Crocker PR and van Aalten DM. High resolution crystal structures of Siglec-7. Insights into ligand specificity in the Siglec family. *J Biol Chem*. 2003;278:3372-3377.
53. Attrill H, Takazawa H, Witt S, Kelm S, Isecke R, Brossmer R, Ando T, Ishida H, Kiso M, Crocker PR and van Aalten DM. The structure of siglec-7 in complex with sialosides: leads for rational structure-based inhibitor design. *Biochem J*. 2006;397:271-278.
54. Attrill H, Imamura A, Sharma RS, Kiso M, Crocker PR and van Aalten DM. Siglec-7 undergoes a major conformational change when complexed with the alpha(2,8)-disialylganglioside GT1b. *J Biol Chem*. 2006;281:32774-83.
55. Hsieh FL, Turner L, Bolla JR, Robinson CV, Lavstsen T and Higgins MK. The structural basis for CD36 binding by the malaria parasite. *Nat Commun*. 2016;7:12837.
56. Maekawa S, Ohto U, Shibata T, Miyake K and Shimizu T. Crystal structure of NOD2 and its implications in human disease. *Nat Commun*. 2016;7:11813.

57. Chadwick AC, Jensen DR, Hanson PJ, Lange PT, Proudfoot SC, Peterson FC, Volkman BF and Sahoo D. NMR Structure of the C-Terminal Transmembrane Domain of the HDL Receptor, SR-BI, and a Functionally Relevant Leucine Zipper Motif. *Structure*. 2017;25:446-457.
58. Kocher O, Birrane G, Yesilaltay A, Shechter S, Pal R, Daniels K and Krieger M. Identification of the PDZ3 domain of the adaptor protein PDZK1 as a second, physiologically functional binding site for the C terminus of the high density lipoprotein receptor scavenger receptor class B type I. *J Biol Chem*. 2011;286:25171-25186.
59. Paddock C, Lytle BL, Peterson FC, Holyst T, Newman PJ, Volkman BF and Newman DK. Residues within a lipid-associated segment of the PECAM-1 cytoplasmic domain are susceptible to inducible, sequential phosphorylation. *Blood*. 2011;117:6012-6023.
60. Paddock C, Zhou D, Lertkiatmongkol P, Newman PJ and Zhu J. Structural basis for PECAM-1 homophilic binding. *Blood*. 2016;127:1052-1061.
61. Hu M, Zhang H, Liu Q and Hao Q. Structural Basis for Human PECAM-1-Mediated Trans-homophilic Cell Adhesion. *Sci Rep*. 2016;6:38655.
62. Parang K, Till JH, Ablooglu AJ, Kohanski RA, Hubbard SR and Cole PA. Mechanism-based design of a protein kinase inhibitor. *Nat Struct Biol*. 2001;8:37-41.
63. Till JH, Ablooglu AJ, Frankel M, Bishop SM, Kohanski RA and Hubbard SR. Crystallographic and solution studies of an activation loop mutant of the insulin receptor tyrosine kinase: insights into kinase mechanism. *J Biol Chem*. 2001;276:10049-10055.
64. Hubbard SR. Crystal structure of the activated insulin receptor tyrosine kinase in complex with peptide substrate and ATP analog. *EMBO J*. 1997;16:5572-5581.
65. Hubbard SR, Wei L, Ellis L and Hendrickson WA. Crystal structure of the tyrosine kinase domain of the human insulin receptor. *Nature*. 1994;372:746-754.
66. Li S, Covino ND, Stein EG, Till JH and Hubbard SR. Structural and biochemical evidence for an autoinhibitory role for tyrosine 984 in the juxtamembrane region of the insulin receptor. *J Biol Chem*. 2003;278:26007-26014.
67. Hu J, Liu J, Ghirlando R, Saltiel AR and Hubbard SR. Structural basis for recruitment of the adaptor protein APS to the activated insulin receptor. *Mol Cell*. 2003;12:1379-1389.
68. Depetris RS, Hu J, Gimpelevich I, Holt LJ, Daly RJ and Hubbard SR. Structural basis for inhibition of the insulin receptor by the adaptor protein Grb14. *Mol Cell*. 2005;20:325-333.
69. Li S, Depetris RS, Barford D, Chernoff J and Hubbard SR. Crystal structure of a complex between protein tyrosine phosphatase 1B and the insulin receptor tyrosine kinase. *Structure*. 2005;13:1643-1651.
70. Lou M, Garrett TP, McKern NM, Hoyne PA, Epa VC, Bentley JD, Lovrecz GO, Cosgrove LJ, Frenkel MJ and Ward CW. The first three domains of the insulin receptor differ structurally from the insulin-like growth factor 1 receptor in the regions governing ligand specificity. *Proc. Natl. Acad. Sci. U.S.A.* 2006;103:12429-12434.

71. Li Q, Wong YL and Kang C. Solution structure of the transmembrane domain of the insulin receptor in detergent micelles. *Biochim Biophys Acta*. 2014;1838:1313-1321.
72. Katayama N, Orita M, Yamaguchi T, Hisamichi H, Kuromitsu S, Kurihara H, Sakashita H, Matsumoto Y, Fujita S and Niimi T. Identification of a key element for hydrogen-bonding patterns between protein kinases and their inhibitors. *Proteins*. 2008;73:795-801.
73. Wu J, Tseng YD, Xu CF, Neubert TA, White MF and Hubbard SR. Structural and biochemical characterization of the KRLB region in insulin receptor substrate-2. *Nat Struct Mol Biol*. 2008;15:251-258.
74. Chamberlain SD, Wilson JW, Deanda F, Patnaik S, Redman AM, Yang B, Shewchuk L, Sabbatini P, Leesnitzer MA, Groy A, Atkins C, Gerding R, Hassell AM, Lei H, Mook RA, Jr., Moorthy G, Rowand JL, Stevens KL, Kumar R and Shotwell JB. Discovery of 4,6-bis-anilino-1H-pyrrolo[2,3-d]pyrimidines: potent inhibitors of the IGF-1R receptor tyrosine kinase. *Bioorg Med Chem Lett*. 2009;19:469-473.
75. Patnaik S, Stevens KL, Gerding R, Deanda F, Shotwell JB, Tang J, Hamajima T, Nakamura H, Leesnitzer MA, Hassell AM, Shewchuck LM, Kumar R, Lei H and Chamberlain SD. Discovery of 3,5-disubstituted-1H-pyrrolo[2,3-b]pyridines as potent inhibitors of the insulin-like growth factor-1 receptor (IGF-1R) tyrosine kinase. *Bioorg Med Chem Lett*. 2009;19:3136-3140.
76. Menting JG, Whittaker J, Margetts MB, Whittaker LJ, Kong GK, Smith BJ, Watson CJ, Zakova L, Kletvikova E, Jiracek J, Chan SJ, Steiner DF, Dodson GG, Brzozowski AM, Weiss MA, Ward CW and Lawrence MC. How insulin engages its primary binding site on the insulin receptor. *Nature*. 2013;493:241-245.
77. Cabail MZ, Li S, Lemmon E, Bowen ME, Hubbard SR and Miller WT. The insulin and IGF1 receptor kinase domains are functional dimers in the activated state. *Nat Commun*. 2015;6:6406.
78. Menting JG, Lawrence CF, Kong GK, Margetts MB, Ward CW and Lawrence MC. Structural Congruency of Ligand Binding to the Insulin and Insulin/Type 1 Insulin-like Growth Factor Hybrid Receptors. *Structure*. 2015;23:1271-1282.
79. Croll TI, Smith BJ, Margetts MB, Whittaker J, Weiss MA, Ward CW and Lawrence MC. Higher-Resolution Structure of the Human Insulin Receptor Ectodomain: Multi-Modal Inclusion of the Insert Domain. *Structure*. 2016;24:469-476.
80. Sanderson MP, Apgar J, Garin-Chesa P, Hofmann MH, Kessler D, Quant J, Savchenko A, Schaaf O, Treu M, Tye H, Zahn SK, Zoephel A, Haaksma E, Adolf GR and Kraut N. BI 885578, a Novel IGF1R/INSR Tyrosine Kinase Inhibitor with Pharmacokinetic Properties That Dissociate Antitumor Efficacy and Perturbation of Glucose Homeostasis. *Mol Cancer Ther*. 2015;14:2762-2772.
81. Stauffer F, Cowan-Jacob SW, Scheufler C and Furet P. Identification of a 5-[3-phenyl-(2-cyclic-ether)-methylether]-4-aminopyrrolo[2,3-d]pyrimidine series of IGF-1R inhibitors. *Bioorg Med Chem Lett*. 2016;26:2065-2067.
82. Lawrence CF, Margetts MB, Menting JG, Smith NA, Smith BJ, Ward CW and Lawrence MC. Insulin Mimetic Peptide Disrupts the Primary Binding Site of the Insulin Receptor. *J Biol Chem*. 2016;291:15473-15481.
83. Cai W, Sakaguchi M, Kleinridders A, Gonzalez-Del Pino G, Dreyfuss JM, O'Neill BT, Ramirez AK, Pan H, Winnay JN,

Boucher J, Eck MJ and Kahn CR. Domain-dependent effects of insulin and IGF-1 receptors on signalling and gene expression. *Nat Commun*. 2017;8:14892.
84. Anastassiadis T, Duong-Ly KC, Deacon SW, Lafontant A, Ma H, Devarajan K, Dunbrack RL, Jr., Wu J and Peterson JR. A highly selective dual insulin receptor (IR)/insulin-like growth factor 1 receptor (IGF-1R) inhibitor derived from an extracellular signal-regulated kinase (ERK) inhibitor. *J Biol Chem*. 2013;288:28068-28077.
85. Menting JG, Yang Y, Chan SJ, Phillips NB, Smith BJ, Whittaker J, Wickramasinghe NP, Whittaker LJ, Pandyarajan V, Wan ZL, Yadav SP, Carroll JM, Strokes N, Roberts CT, Jr., Ismail-Beigi F, Milewski W, Steiner DF, Chauhan VS, Ward CW, Weiss MA and Lawrence MC. Protective hinge in insulin opens to enable its receptor engagement. *Proc. Natl. Acad. Sci. U.S.A.* 2014;111:E3395-3404.
86. Carpenter B, Hemsworth GR, Wu Z, Maamra M, Strasburger CJ, Ross RJ and Artymiuk PJ. Structure of the human obesity receptor leptin-binding domain reveals the mechanism of leptin antagonism by a monoclonal antibody. *Structure*. 2012;20:487-497.
87. Gattis JL, Washington AV, Chisholm MM, Quigley L, Szyk A, McVicar DW and Lubkowski J. The structure of the extracellular domain of triggering receptor expressed on myeloid cells like transcript-1 and evidence for a naturally occurring soluble fragment. *J Biol Chem*. 2006;281:13396-13403.
88. Leppanen VM, Saharinen P and Alitalo K. Structural basis of Tie2 activation and Tie2/Tie1 heterodimerization. *Proc. Natl. Acad. Sci. U.S.A.* 2017;114:4376-4381.
89. Yan Q, Malashkevich VN, Fedorov A, Fedorov E, Cao E, Lary JW, Cole JL, Nathenson SG and Almo SC. Structure of CD84 provides insight into SLAM family function. *Proc. Natl. Acad. Sci. U.S.A.* 2007;104:10583-10588.
90. Karthikeyan S, Leung T and Ladias JA. Structural determinants of the Na+/H+ exchanger regulatory factor interaction with the beta 2 adrenergic and platelet-derived growth factor receptors. *J Biol Chem*. 2002;277:18973-18978.
91. Pauptit RA, Dennis CA, Derbyshire DJ, Breeze AL, Weston SA, Rowsell S and Murshudov GN. NMR trial models: experiences with the colicin immunity protein Im7 and the p85alpha C-terminal SH2-peptide complex. *Acta Crystallogr D Biol Crystallogr*. 2001;57:1397-1404.
92. Waksman G, Kominos D, Robertson SC, Pant N, Baltimore D, Birge RB, Cowburn D, Hanafusa H, Mayer BJ, Overduin M, Resh MD, Rios CB, Silverman L and Kuriyan J. Crystal structure of the phosphotyrosine recognition domain SH2 of v-src complexed with tyrosine-phosphorylated peptides. *Nature*. 1992;358:646-653.
93. Muhle-Goll C, Hoffmann S, Afonin S, Grage SL, Polyansky AA, Windisch D, Zeitler M, Burck J and Ulrich AS. Hydrophobic matching controls the tilt and stability of the dimeric platelet-derived growth factor receptor (PDGFR) beta transmembrane segment. *J Biol Chem*. 2012;287:26178-26186.
94. Pascal SM, Singer AU, Gish G, Yamazaki T, Shoelson SE, Pawson T, Kay LE and Forman-Kay JD. Nuclear magnetic resonance structure of an SH2 domain of phospholipase C-gamma 1 complexed with a high affinity binding peptide. *Cell*. 1994;77:461-472.

95. Shim AH, Liu H, Focia PJ, Chen X, Lin PC and He X. Structures of a platelet-derived growth factor/propeptide complex and a platelet-derived growth factor/receptor complex. *Proc. Natl. Acad. Sci. U.S.A.* 2010;107:11307-11312.

Supplemental Figure S1

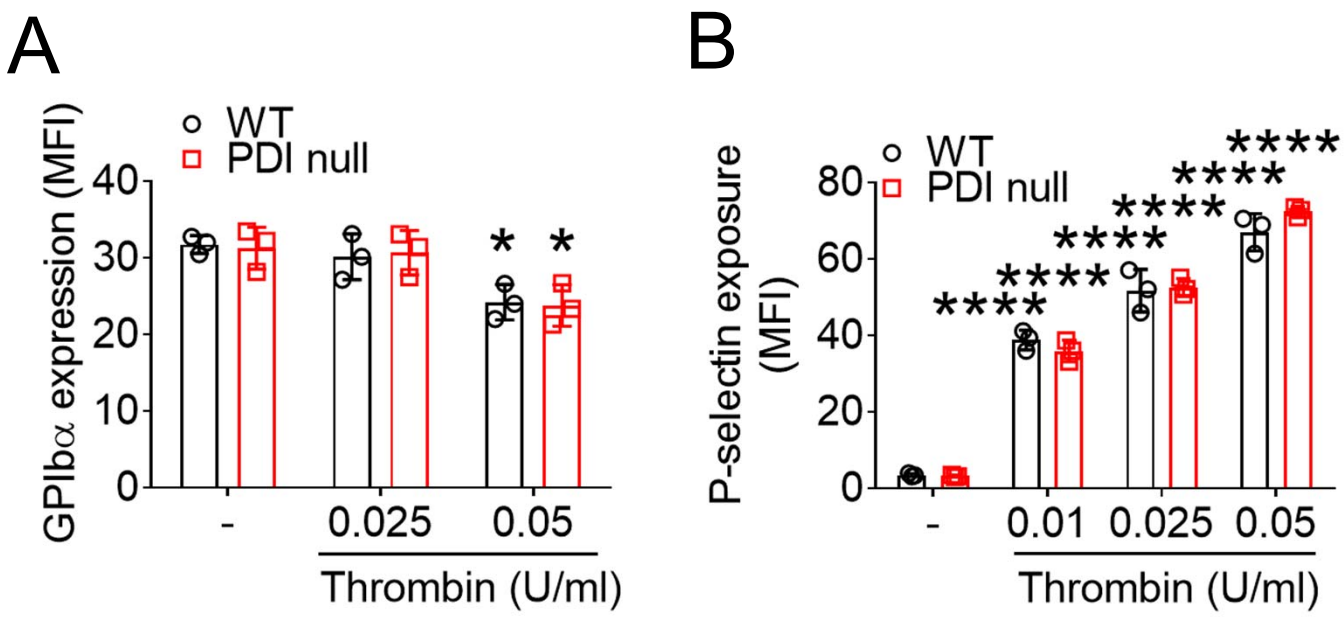

Supplemental Figure S2

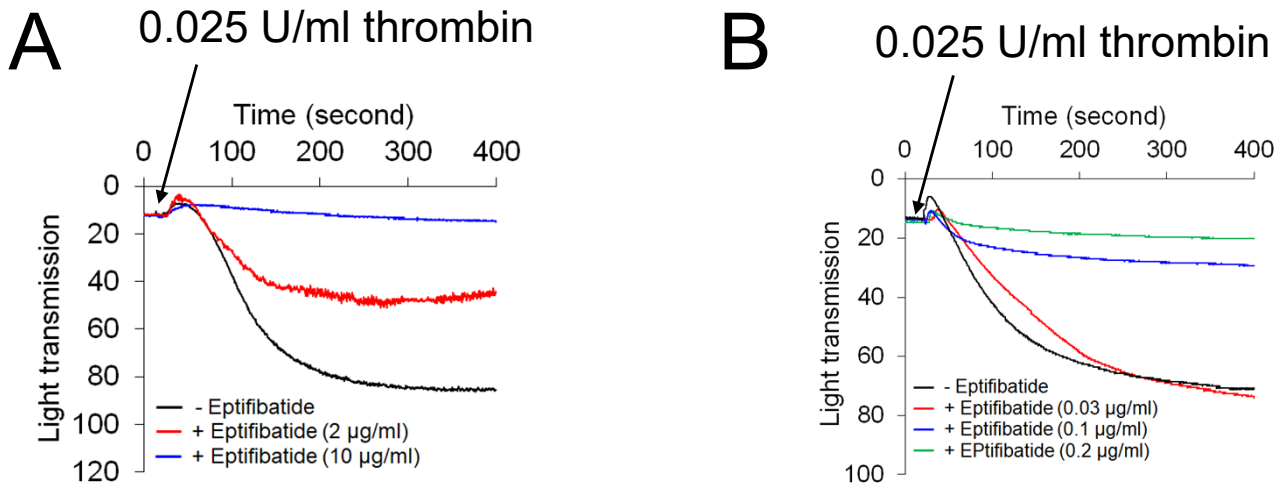

Supplemental Figure S3

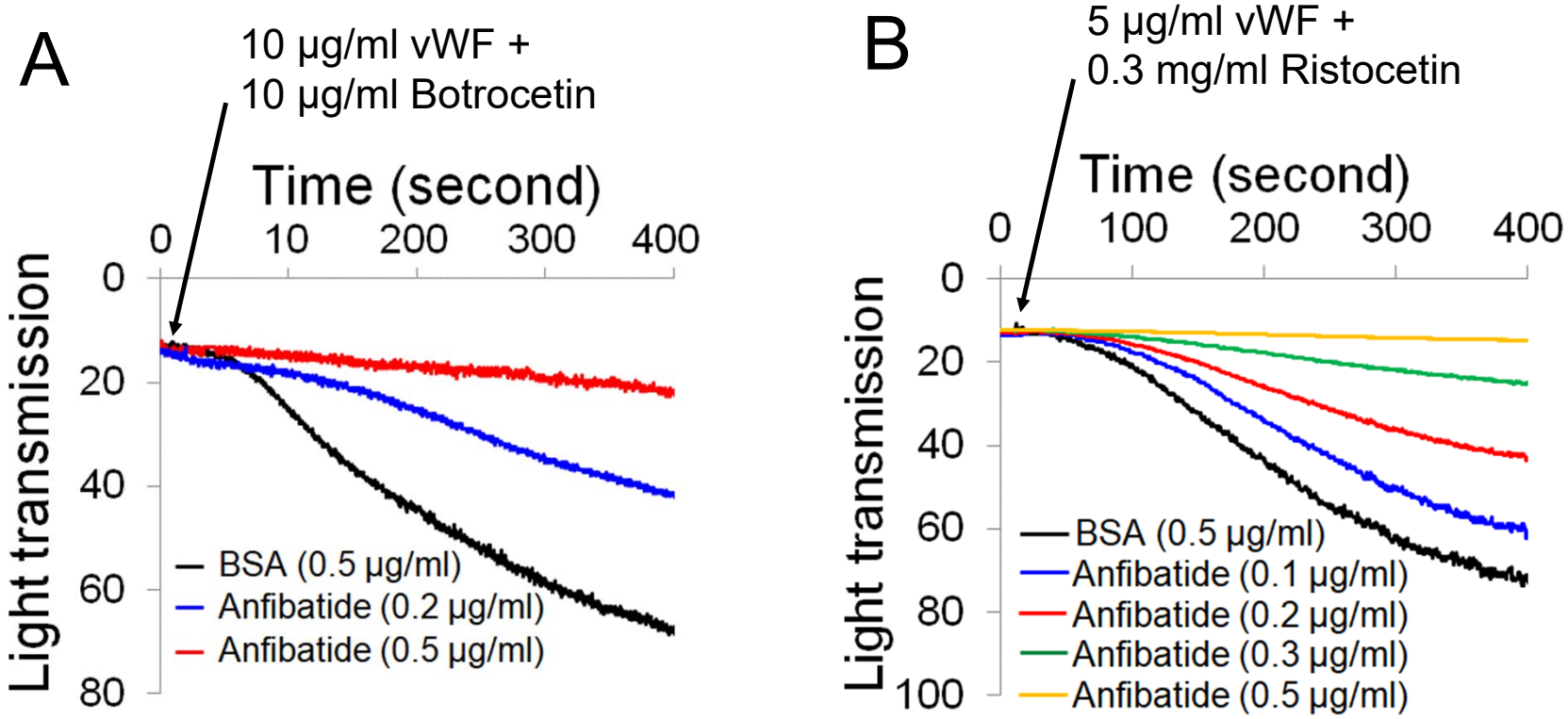

Supplemental Figure S4

A

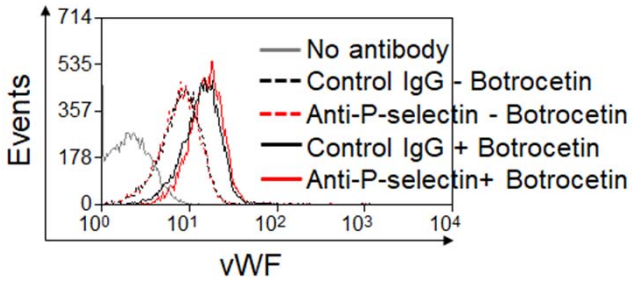

B

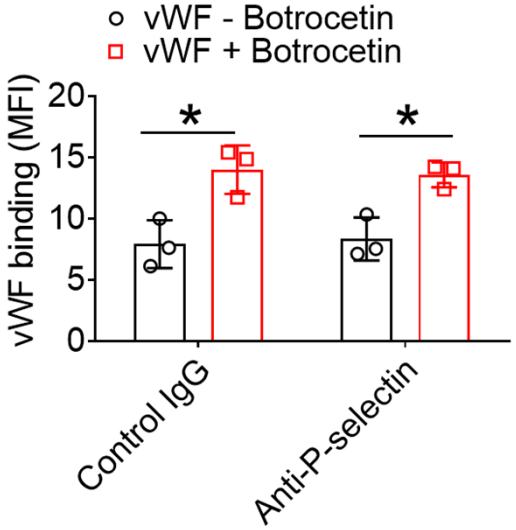

Supplemental Figure S5

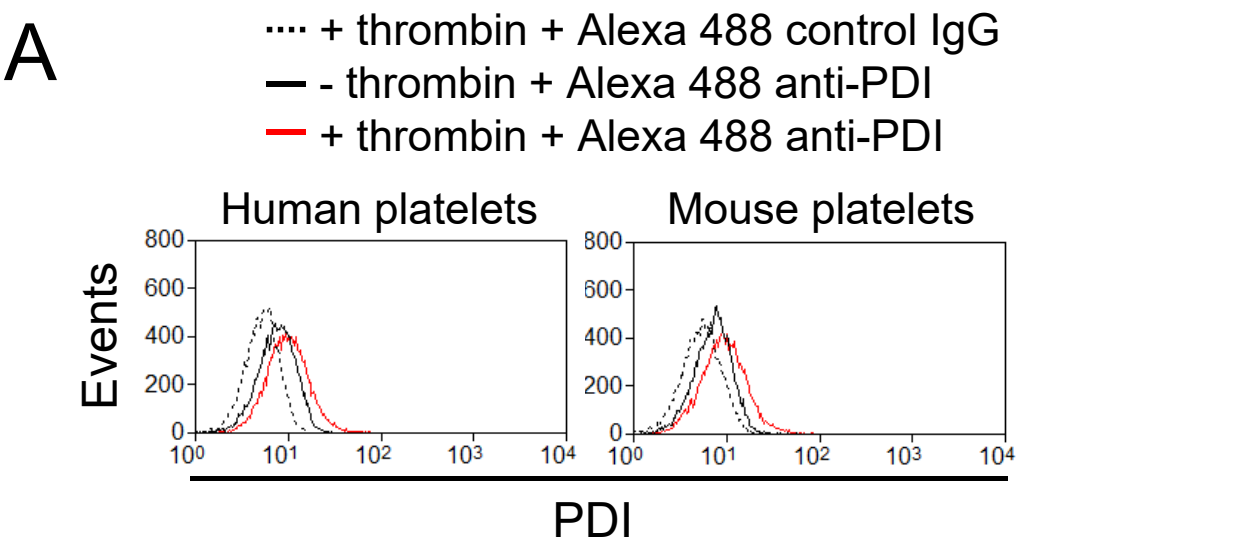

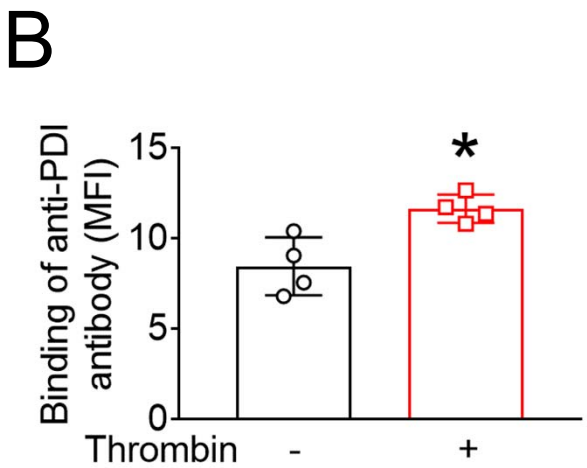

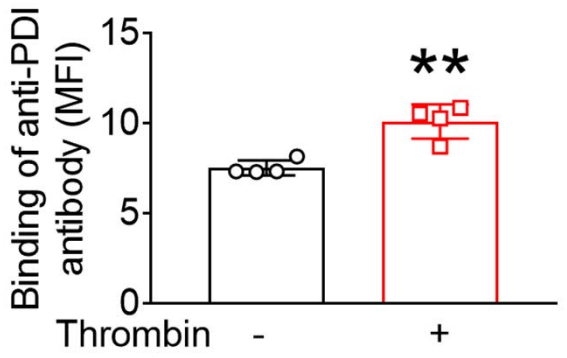

Supplemental Figure S6

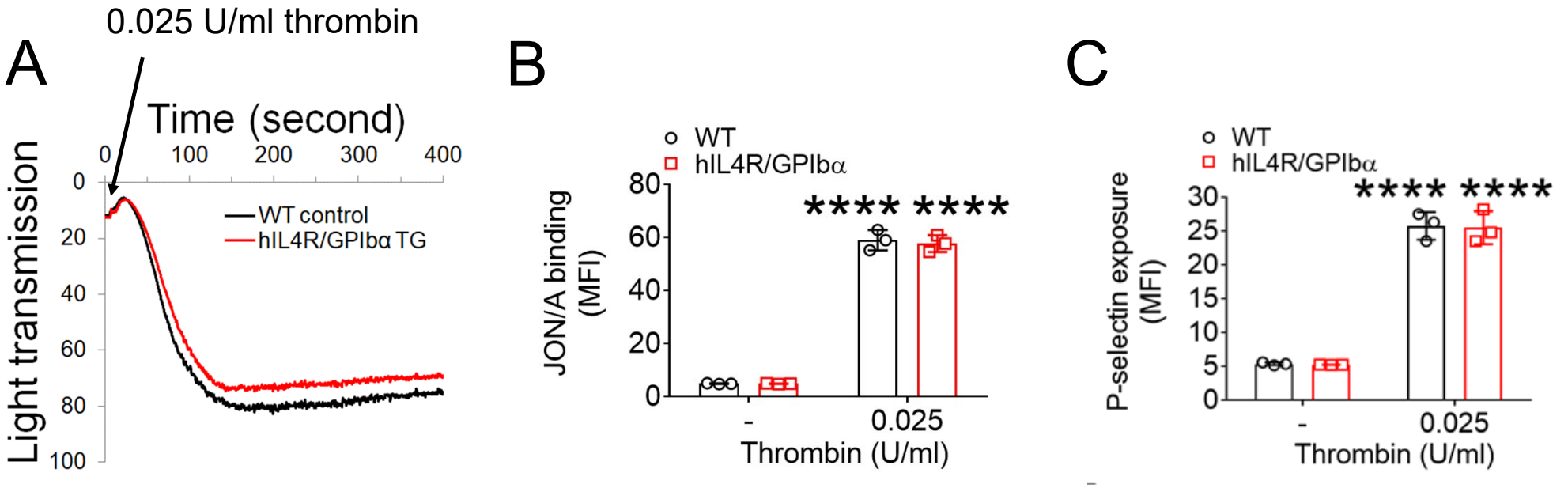

Supplemental Figure S7

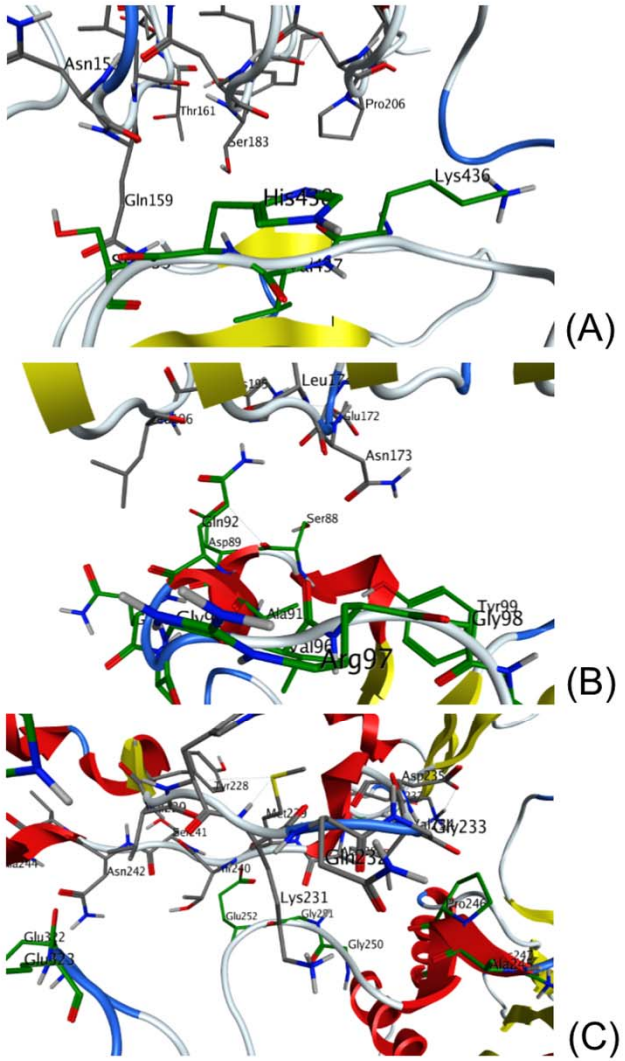

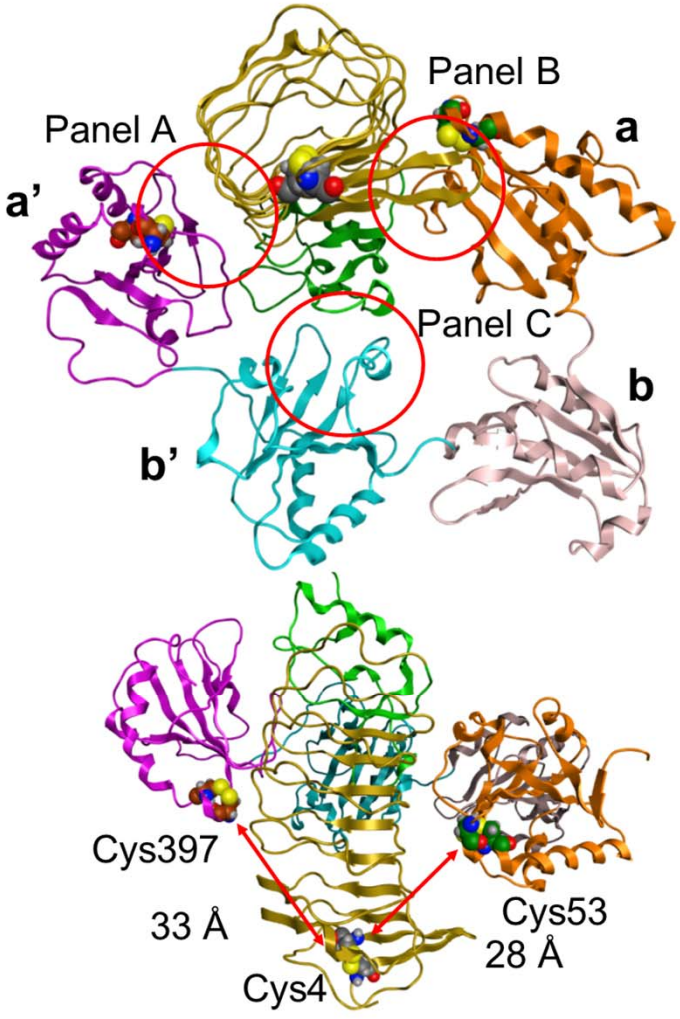

Supplemental Figure S8

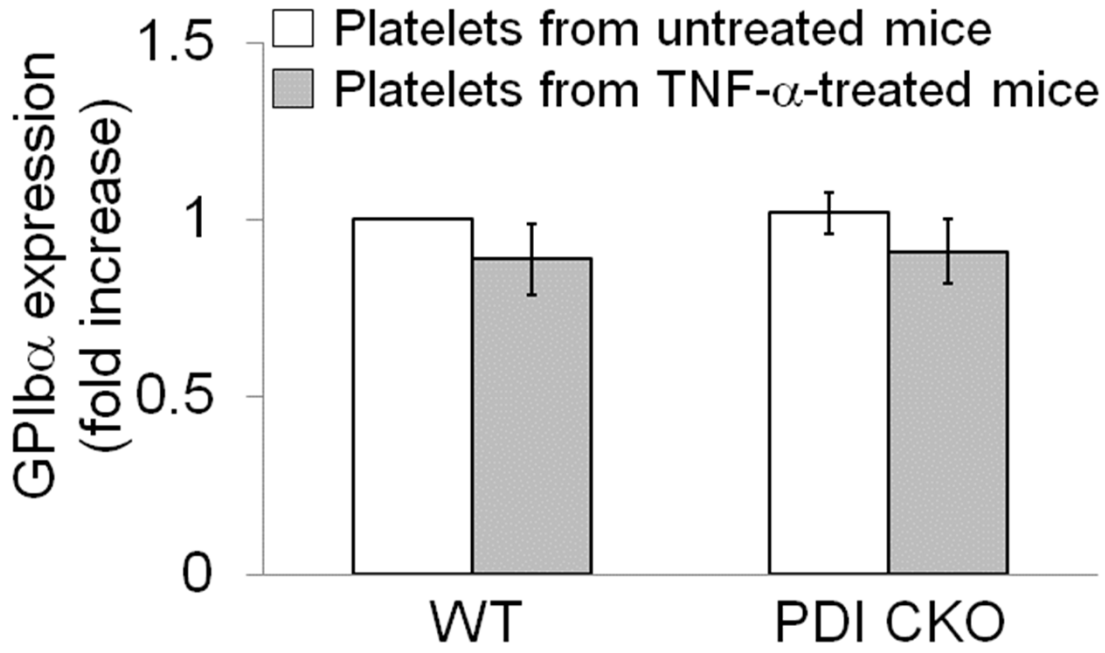

Supplemental Figure S9

A

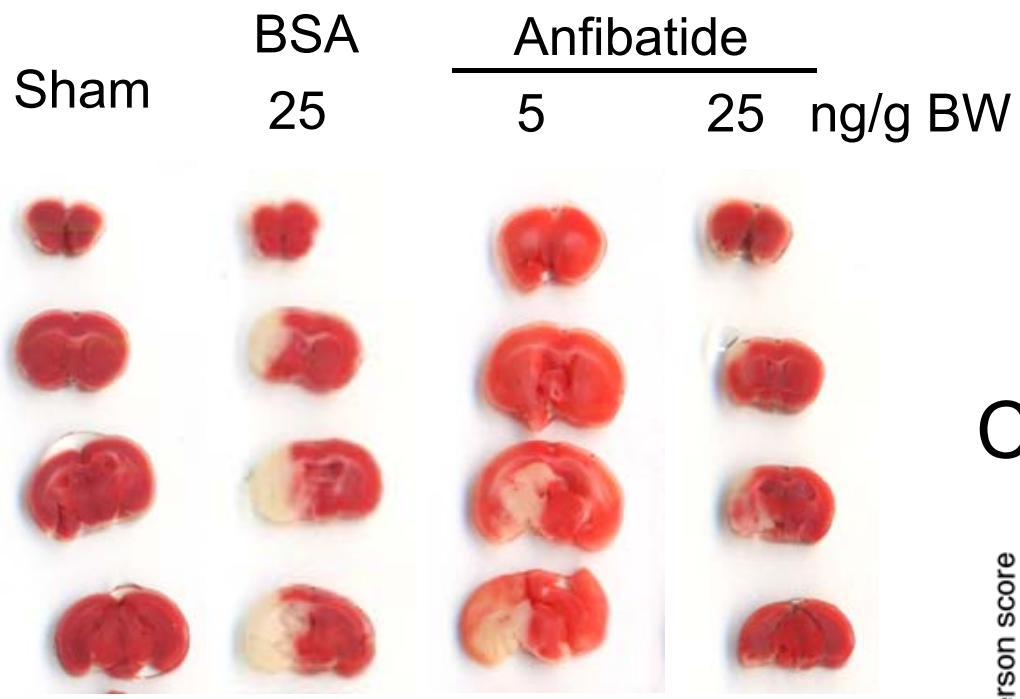

B

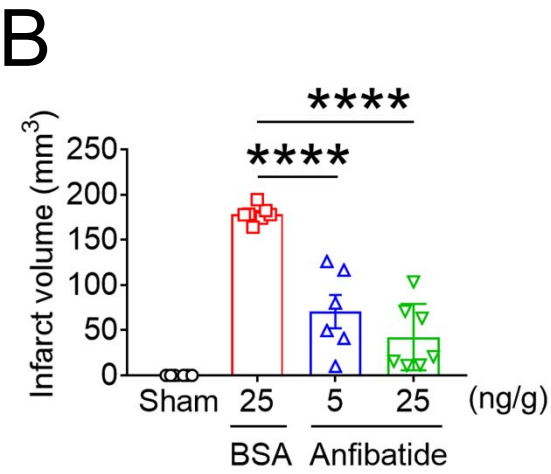

C

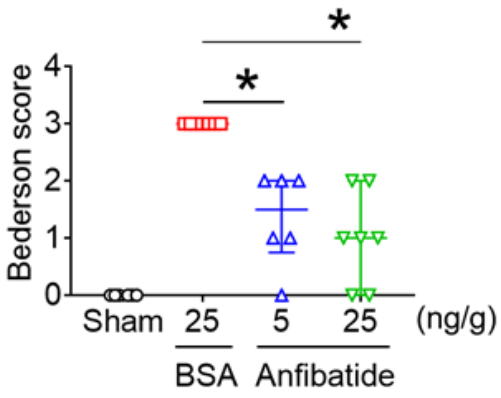

D

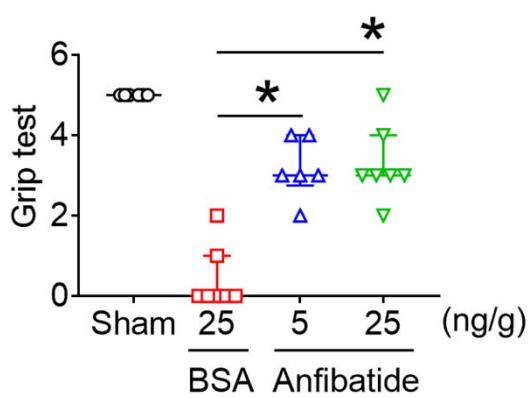

Supplemental Figure S10

A

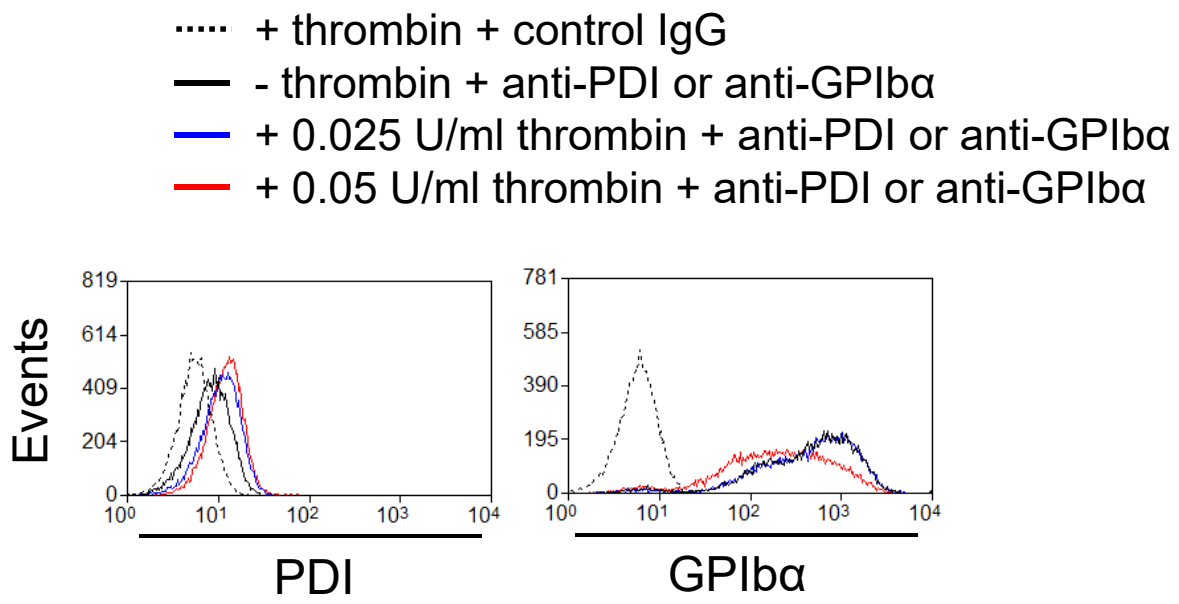

B

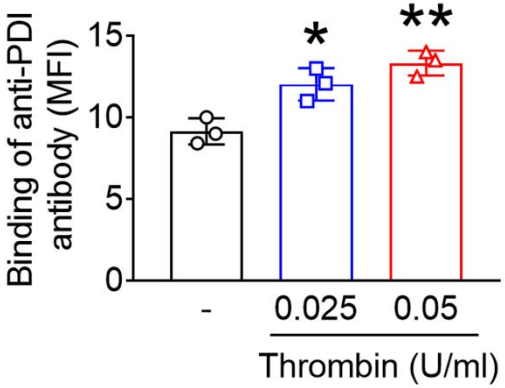

C

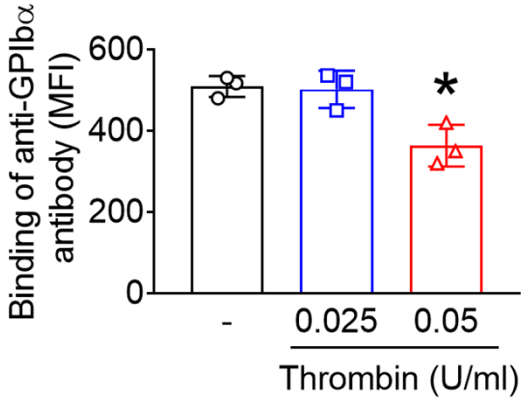

Supplemental Figure S11

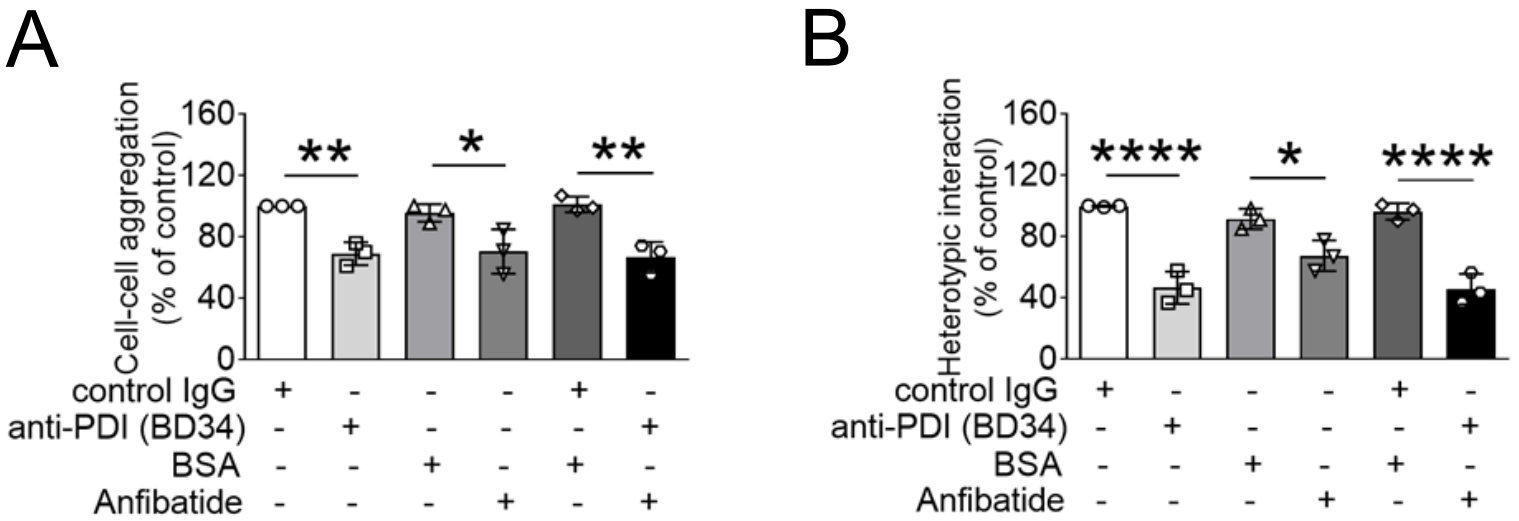

Supplemental Figure S12

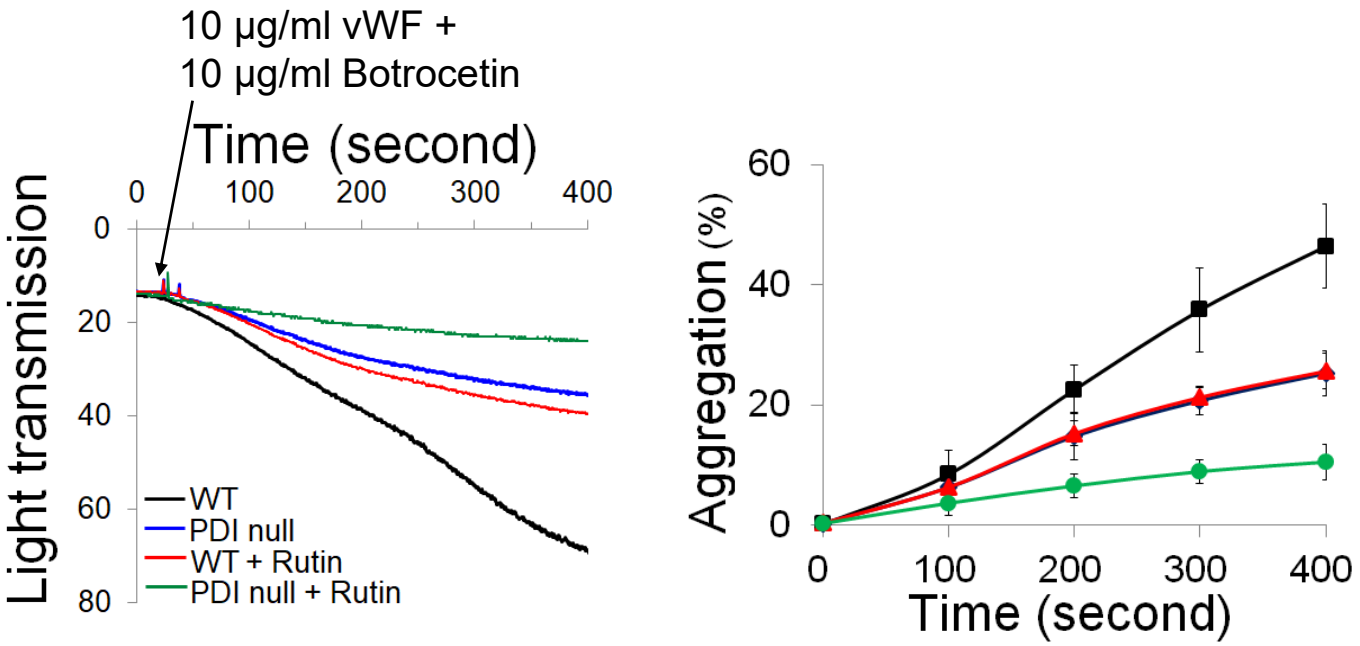

SUPPLEMENTAL FIGURE LEGEND

Figure S1. The surface levels of platelet GPIbα and P-selectin are not affected by PDI deletion. Flow cytometry was performed to determine the surface amount of GPIbα (A) and P-selectin (B) on resting and thrombin-activated WT and PDI-null platelets. Data are shown as the MFI value and represent the mean ± SD (n = 3). *P < 0.05 and ****P < 0.0001 versus unstimulated platelets after ANOVA and Dunnett's test.

Figure S2. Eptifibatide blocks αIIbβ3-mediated platelet aggregation induced by thrombin. WT mouse (A) and human (B) platelets were pretreated with vehicle or different concentrations of eptifibatide, followed by stimulation with thrombin. The representative aggregation traces were obtained from three independent experiments.

Figure S3. Anfibatide inhibits platelet agglutination in a concentration-dependent manner. Mouse (A) and human (B) platelets were pretreated with BSA (0.5 μg/ml) or Anfibatide (0.1-0.5 μg/ml) and then incubated with vWF and either botrocetin or ristocetin. The representative agglutination traces were obtained from three independent experiments.

Figure S4. Inhibition of P-selectin does not impair vWF binding to mouse platelets. WT mouse platelets were pretreated with control IgG or a blocking anti-P-selectin antibody (10 μg/ml). After washing, platelets were incubated with 10 μg/ml vWF and 10 mM EDTA in the presence or absence of 10 μg/ml botrocetin. Flow cytometry was performed using FITC-labeled anti-vWF antibodies. (A) Representative histogram. (B) Data are shown as the MFI value and represent the mean ± SD (n = 3). *P < 0.05 after

ANOVA and Tukey's test.

Figure S5. Surface-bound PDI is detected on unstimulated and stimulated platelets. WT control mouse ($PDI^{flox/flox}$, A-B) and human (A and C) platelets were treated with or without 0.025 U/ml thrombin. The surface level of PDI was measured by flow cytometry using rabbit IgG or polyclonal anti-PDI antibodies equivalently conjugated with Alexa Fluor 488. Data represent the mean ± SD (n = 4). *P < 0.05 or **P < 0.01 versus unstimulated platelets after Student's t-test.

Figure S6. Deletion of the GPIbα extracellular domain does not affect aggregation, αIIbβ3 activation, and P-selectin exposure in platelets. (A) Aggregation of WT and hIL4R/GPIbα platelets was initiated with 0.025 U/ml thrombin. The representative aggregation trace was obtained from three independent experiments. (B-C) WT and hIL4R/GPIbα platelets were treated with or without 0.025 U/ml thrombin, followed by flow cytometry using antibodies against activated αIIbβ3 (JON/A) or P-selectin. Data represent the mean ± SD (n = 3). ****P < 0.0001 versus unstimulated platelets after Student's t-test.

Figure S7. A docking model of PDI-GPIbα complex. A set of representative residues at the interface between GPIbα and oxidized PDI. Panel A: the a'-domain of PDI and the β-finger of GPIbα, Panel B: the a-domain of PDI and the β-finger of GPIbα, and Panel C: the b'-domain of PDI and the β-switch of GPIbα.

Figure S8. GPIbα is not shed in circulating platelets during TNF-α-induced vascular

inflammation. Saline or TNF-α was intrascrotally injected into WT and platelet-specific PDI CKO mice. Platelets were isolated at 3 hours after TNF-α injection. The surface level of GPIbα was measured by flow cytometry. Data represent the mean ± SD (n = 3 mice per group).

Figure S9. Anfibatide dose-dependently reduces the infarct volume and ameliorates neurological deficits in I/R-induced stroke. WT (C57BL/6) mice were subjected to transient MCAO and reperfusion as described in Methods. BSA or Anfibatide (5 or 25 ng/g BW) was intravenously infused into mice right after 1-hour MCAO, followed by 23-hour reperfusion. (A) Staining of brain sections with 2,3,5-triphenyltetrazolium chloride. (B) The infarct volume was measured. (C-D) The Bederson score and grip test were used to analyze neurologic outcome in the surviving animals 24 hours after MCAO. Data represent the mean ± SD except for the Bederson score and the grip test score, which are shown as scatter plots including median with interquartile range (n = 6-7 mice per group). *:P<0.05 or ****:P<0.0001 after ANOVA and Tukey's test (B) or Kruskal-Wallis test with post hoc Dunn correction (C-D).

Figure S10. GPIbα and PDI are detected on unstimulated and stimulated platelets isolated from SCD mice. Platelets isolated from SCD mice were treated with or without 0.025-0.05 U/ml thrombin. The surface levels of GPIbα and PDI were measured by flow cytometry using Alexa Fluor 488-conjugated rabbit IgG or polyclonal anti-PDI antibodies, or FITC-conjugated rat IgG2a or anti-GPIbα antibodies (Xia.B2). (A) Representative histogram. (B-C) Data are shown as the MFI value and represent the mean ± SD (n = 3).

*P < 0.05 or **P < 0.01 versus unstimulated platelets after ANOVA and Dunnett's test.

Figure S11. Platelet PDI-regulated GPIbα function is important for heterotypic aggregation of platelets and neutrophils isolated from SCD mice. Platelets and neutrophils were isolated from SCD mice and labeled with DyLight 488-conjugated CD42c and Alexa Fluor 647-conjugated anti-Ly-6G antibodies, respectively. Platelets were treated with 0.025 U/ml thrombin in the presence of control IgG, an anti-PDI antibody, BSA, Anfibatide, or both inhibitors, followed by mixing with activated neutrophils under a stirring condition. Flow cytometry was performed as shown in Figure 4A-C. Cell-cell aggregation was measured by (A) the number of cell-cell aggregates and (B) the fluorescence intensities of anti-CD42c antibodies (Heterotypic interaction). *:P<0.05, **:P<0.01, or ****:P<0.0001 after ANOVA and Tukey's test.

Figure S12. Rutin inhibits agglutination of PDI-null platelets. WT and PDI-null platelets were pre-incubated with vehicle (0.1% DMSO) or 50 μM rutin and then treated with vWF and botrocetin. The representative agglutination/aggregation traces were obtained from three independent experiments. Data represent the mean ± SD.

Video 1. Platelet-neutrophil interactions during TNF-α-induced vascular inflammation in WT mice.

Video 2. Platelet-neutrophil interactions during TNF-α-induced vascular inflammation in platelet-specific PDI CKO mice.

Video 3. Platelet-neutrophil interactions during TNF-α-induced vascular inflammation in platelet-specific PDI CKO mice treated with wtPDI.

Video 4. Platelet-neutrophil interactions during TNF-α-induced vascular inflammation in platelet-specific PDI CKO mice treated with dmPDI.